UNITED STATES DEPARTMENT OF THE INTERIOR

GEOLOGICAL SURVEY

# Age and Petrology of the Tertiary As Sarat Volcanic Field, Southwestern Saudi Arabia

By

Edward A. duBray[1], Douglas B. Stoeser[1], and Edwin H. McKee[1]

Open-File Report 91- 148

Report prepared by the U.S. Geological Survey in cooperation with the Deputy Ministry for Mineral Resources, Saudi Arabia



1991

# CONTENTS



## TABLES

## TABLES (Continued)



## FIGURES

# AGE AND PETROLOGY OF THE TERTIARY AS SARAT VOLCANIC FIELD, SOUTHWESTERN SAUDI ARABIA

By
**Edward A. du Bray, Douglas B. Stoeser, and Edwin H. McKee**

## ABSTRACT

Harrat As Sarat forms the second smallest and southernmost of the basalt fields of western Saudi Arabia and is part of a voluminous Red Sea rift-related continental alkali basalt province. The rocks of the As Sarat were emplaced during the first stage of Red Sea rifting and represent the northernmost extension of the Tertiary Trap Series volcanics that occur mainly in the Yemen Arab Republic and Ethiopia. The field consists of up to 580 m of basalt flows, that are intruded by basaltic plugs, necks, minor dikes, and highly evolved peralkaline trachyte intrusions. K-Ar ages indicate that the As Sarat field formed between 31 and 22 Ma and contains an eruption hiatus of one million years that began about 25 Ma. Pre-hiatus flows are primarily hypersthene normative intersertal subalkaline basalt, whereas the majority of post-hiatus flows are nepheline normative alkali basalt and hawaiite with trachytic textures. Normative compositions of the basalts are consistent with their genesis by partial melting at varying depths. Trace element abundances in the basalt indicate that varying degrees of partial melting and fractional crystallization (or crystal accumulation) had major and minor roles, respectively, in development of compositional variation in these rocks. Modeling indicates that the pre-hiatus subalkaline basalts represent 8.10 percent mantle melting at depths of about 70 km and the post-hiatus alkali basalts represent 4-9 percent mantle melting at depths greater than 70 km.

## INTRODUCTION

Cenozoic alkali basalt covers about 90,000 $km^2$ in western Saudi Arabia and is part of one of the world's largest alkali basalt provinces (Coleman and others, 1983). These basalts are similar to alkali basalts that occur in the Yemen Arab Republic and across the Red Sea in Ethiopia (Chiesa and others, 1989; and Mohr and Zanettin, 1989); all of these rocks have origins related to Red Sea rifting. Within western Saudi Arabia thirteen alkali basalt fields (harrats) have been delineated (Coleman and others, 1977).

The general characteristics of the Arabian alkali basalts have been described in reconnaissance studies of the region (e.g. Coleman and others, 1983). Several systematic studies of individual Red Sea rift-related basalt fields have been recently completed (Pallister, 1987; Camp and Roobol, 1989). The timing of uplift related to Red Sea rifting is discussed by Bohannon and others (1989), whereas Coleman and

McGuire (1988) and McGuire and Bohannon (1989) describe magma systems and mantle dynamics related to rifting. Hegner and Pallister (1989) present Pb, Sr, and Nd isotopic data for rift volcanics of the central Saudi Arabian coastal plain and infer from these data that magmas represented by these rocks represent mixing of asthenospheric and lithospheric components. Various aspects of the geology of the As Sarat field have been described by Coleman and others (1977), Overstreet and others (1977), Anderson (1979), and Stoeser (1984). Kellogg and Reynolds (1983) conducted a paleomagenetic study of the As Sarat field and identified a reversal within the basalt flow sequence. Their work helps constrain the timing of Red Sea rifting.

Basalt of the As Sarat forms the second smallest (about 750 $km^2$), and most southerly of the Saudi Arabian alkali basalt fields (fig. 1). Exposures extend about 105 km northwestward from a point near the border with the Yemen Arab Republic and are an extension of the Tertiary plateau volcanic fields or Trap Series of Yemen (Capaldi and others, 1983; Chiesa and others, 1989). The field forms a contiguous series of deeply eroded buttes and mesas. The deeply dissected character of the field is a consequence of its lofty position directly east of the Red Sea escarpment. Peaks within the field are as much as 2850 m above sea level and are some of the highest in Saudi Arabia. The field is located about 300 km east of the currently active Red Sea spreading axis and 100 km north of the Tihama Asir complex considered by Coleman and others (1983) to be incipient oceanic crust formed by magmatic activity that accompanied spreading along the Red Sea rift. K-Ar ages presented by Coleman and others (1975, 1983) indicate that the basal and top flows of the As Sarat field were erupted at 30.0±1.0 Ma and 25.3±0.5 Ma, respectively, that two feeder necks were emplaced 24.7±2.0 Ma and 25.4±2.7 Ma, and a trachyte dome at 22.4±0.2 Ma.

The As Sarat field is predominantly underlain by alkali basalt flows that unconformably overlie lateritized rocks of the Late Proterozoic Arabian Shield or Cambro-Ordovician Wajid Sandstone (Overstreet and others, 1977). The field also includes a small number of basaltic necks and basaltic dikes, and five late intrusive trachyte domes that were emplaced at the base of the flows. In the more deeply eroded area north of the As Sarat, numerous Tertiary basalt plugs, as much as 30 m in diameter, occur in an area that extends northwestwards for 65 km in a direction parallel to the Red Sea (fig. 1). These plugs are correlated with the basalts of the As Sarat field and indicate that the areal extent of the field was formerly much greater than at present.

The majority of faults that cut the As Sarat basalts are normal faults that parallel the long axis of the field and the Red Sea margin. These faults are concentrated along the margins of the field and most are down towards the center of the field (Anderson, 1979; Stoeser, 1984). These observations suggest that either the As Sarat basalts were erupted into an active graben or preserved in a graben that post-dates the basalts.

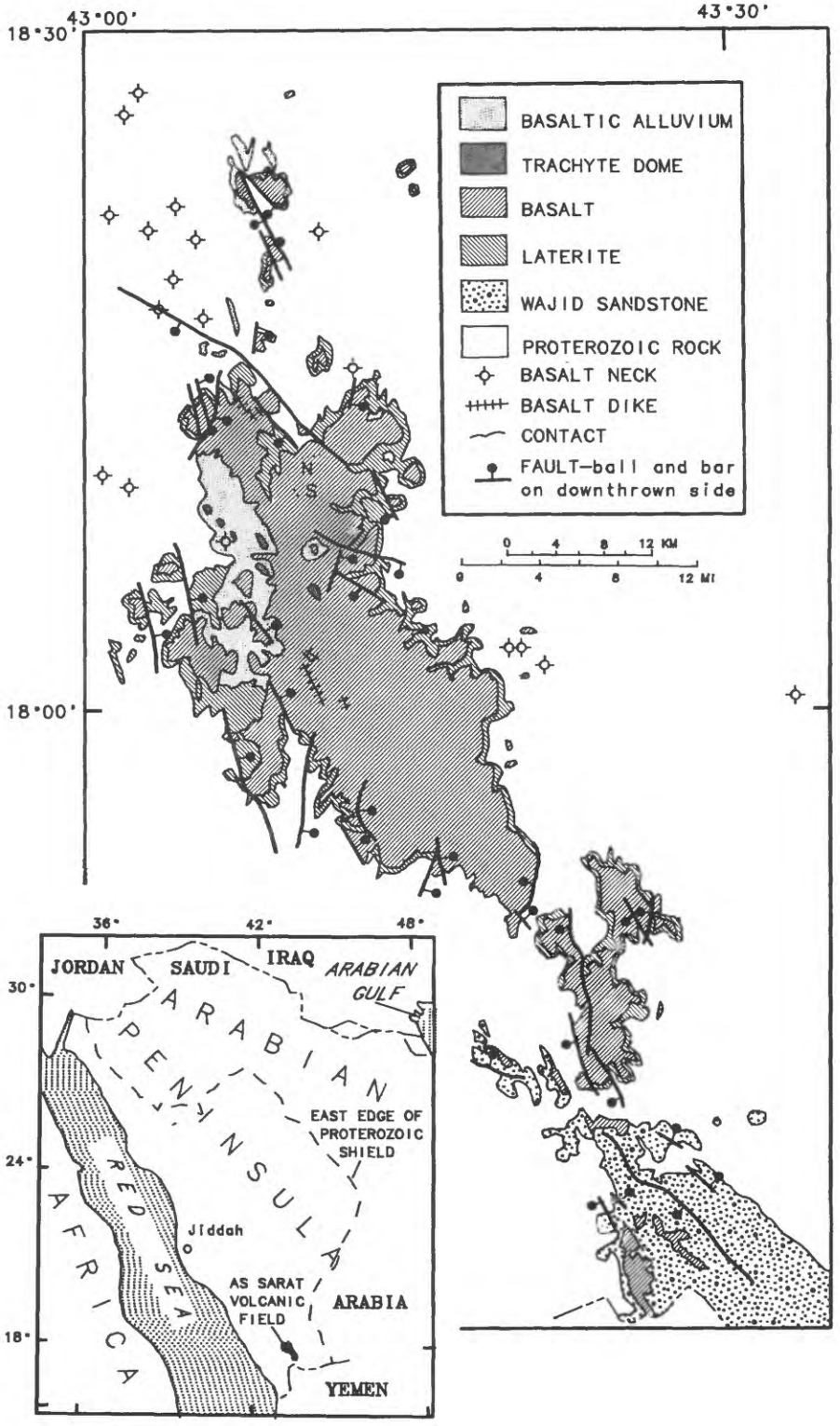


**Figure 1.**—Index and geologic sketch maps (after Anderson, 1979 and Stoeser, 1984) of the As Sarat basalt field, Kingdom of Saudi Arabia. Dotted lines denoted N and S show approximate locations of the northern and southern parts of the Composite Reference Section, respectively.

In order to study the flows of the As Sarat field, a two-part, composite reference section (CRS) in the northern part of the field was chosen for study (figs. 1, 2). The CRS was also included in the study of Kellogg and Reynolds (1983). The lower three-quarters of the CRS forms a ridge located 2.8 km north of a second ridge, where the upper one-quarter of the CRS is exposed. A distinctive thick flow at the top of the lower section and at the base of the upper section permits correlation between the two sections. The maximum total thickness of the CRS is about 580 m. Individual flows are from 3 to 20 meters thick and are at least 35 in number. Flows are mainly composed of massive, fine-grained, poorly to non-vesiculated basalt. Flows display columnar jointing from about their midline to their bases and some are characterized by subhorizontal jointing at their tops. The lower section includes several rather thick intervals composed of friable, scoriaceous basalt. No stratigraphic indicator is present to indicate the top of the basalt sequence and the uppermost flows of the As Sarat field may have been removed by erosion. The absence of well-developed soil horizons and of unconformities indicate that the CRS is an intact sequence, i.e. that no flows have been removed by between-eruption erosional events.

## ACKNOWLEDGMENTS

The field work for this study was performed in accordance with an agreement between the Saudi Arabian Ministry of Petroleum and Mineral Resources and the U.S. Geological Survey (USGS). Reviews by J.S. Pallister, J.C. Ratte, and P. Mohr are much appreciated. Analysts from the Branch of Geochemistry (USGS) are thanked for their efforts.

## ANALYTICAL METHODS

Major oxide and trace element compositions for 28 flows, 4 necks, 4 dikes, and 5 trachyte domes were determined in the Analytical Laboratories of the U.S. Geological Survey (USGS) in Denver, Colorado. Major oxide analyses were performed (analysts, J.E. Taggart, A.I. Bartel, K.C. Stewart, E.C. Robb, and D.F. Siems) using X-ray fluorescence techniques (Taggart and others, 1987), except FeO which was determined (analyst, E. Brandt) by wet chemistry (Jackson and others, 1987). $Fe^{2+}$:$Fe^{3+}$ ratios were adjusted to 9:1 (Ringwood, 1975) and major oxide compositions were recalculated to 100 percent on an anhydrous basis prior to norm calculation and plotting. Co, Cr, Cu, Ni, Sc, V, and Zn abundances were determined (analysts, P.H. Briggs, D.L. Fey, and L.A. Bradley) by inductively coupled plasma-atomic emission spectroscopy (Lichte and others, 1987). Rb, Sr, Y, Zr, Nb, and Ba abundances were determined (by E.A. du Bray) by energy-dispersive X-ray fluorescence spectroscopy (Elsass and du Bray, 1982) using $^{109}Cd$ and $^{241}Am$ radio-isotope excitation sources; these data are considered accurate within 5 percent of the reported abundances. X-ray Assay Laboratories, Ltd. (XRAL), Ontario,

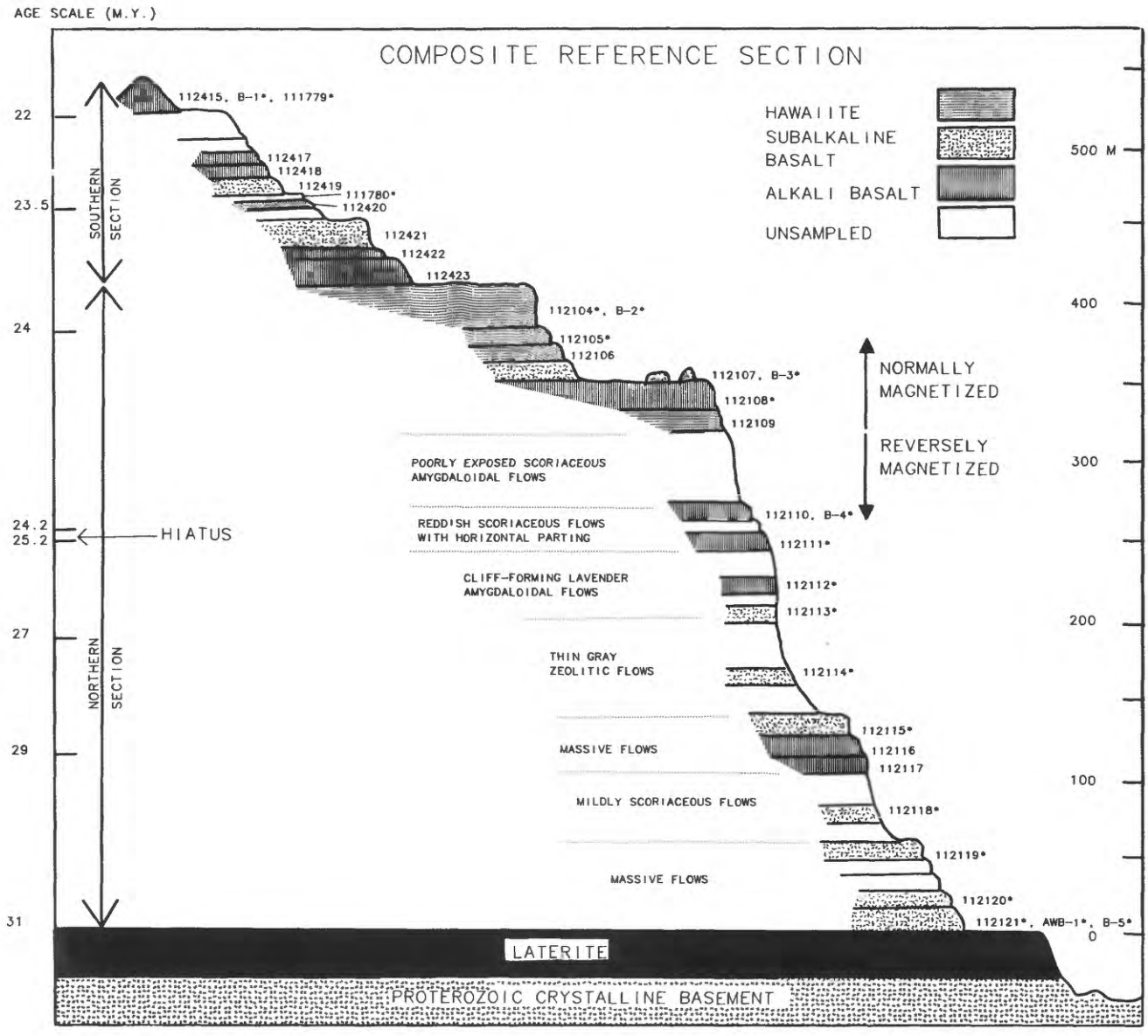


**Figure 2.–Schematic cross section of the composite reference section (CRS). Asterisks following sample numbers indicate dated samples.**

Canada determined rare-earth element (REE) and thorium abundances in samples from 7 flows, 1 neck, 1 dike, and 1 trachyte dome by neutron activation analysis and uranium by delayed neutron counting.

Compositions of feldspar, olivine, and pyroxene were determined using an ARL SEMQ electron microprobe equipped with 6 wavelength dispersive crystal spectrometers. A 5 micron (except feldspars, 25) beam and a 15 kV accelerating voltage with 10 nA sample current were used to make a minimum of three 20-s analyses on three or more grains per sample. Analyzed natural and synthetic minerals were used as standards; all data was reduced using MAGICIV (Colby, 1968).

Sample preparation (for age determinations) and argon and potassium analyses were conducted in USGS laboratories in Menlo Park, California, using techniques described in Dalrymple and Lanphere (1969). Whole rock samples were crushed, sieved to -60 + 100 mesh, washed, and treated for 30 min in 14 percent $HNO_3$ and 1 min in 5 percent HF solutions before loading into a high-vacuum gas-extraction system. Aliquots of the whole rock samples were analyzed for $K_2O$ by a lithium metaborate flux fusion-flame photometry technique; lithium acts as an internal standard (Ingamells, 1970). Argon determinations were made in the USGS isotope geology labs using standard isotope-dilution techniques. Samples of clean argon gas were analyzed using a 600 sector, 15.2 cm-radius, Neir-type mass spectrometer, operated in the static mode. Ages were calculated using the constants of the subcommission on geochronolgy (Steiger and Jager, 1977).

## K–AR GEOCHRONOLOGY

Twenty-two new age determinations on rocks of the As Sarat field are reported (table 1). The dated samples are from flows of the As Sarat volcanic field, with the exception of one age determination for a sample of a trachyte dome. Samples were selected at relatively evenly spaced intervals from the bottom of the CRS to its top in order to determine the duration and frequency of eruptive activity. Basalt flows of the As Sarat volcanic field range in age from about 31 m.y. to about 22 m.y. and the trachyte has an age of about 24 m.y.

Age determinations for two of the samples (nos. 112114 and 112119) have such large analytical uncertainty that they are of no value in age evaluation and three other samples (nos. 112105, 112118, and AWB-1) yield ages that are unreasonable when evaluated with respect to radiometric ages for stratigraphically adjacent flows. These samples appear to be weakly zeolitized, which has affected the isotopic systematics, and thus these data were excluded from our study.

Consideration of stratigraphic relations and age precisions calculated for individual samples allows re-evaluation of age accuracies. The K-Ar determinations

are arranged in stratigraphic succession and shown as bars, the lengths of which represent the limits of analytical uncertainty (precision) at one standard deviation (fig. 3). Because the relative ages of all flows are known from stratigraphy, each radiometric age can be compared with ages for overlying and underlying flows (McKee and Elston, 1980). The patterned areas in figure 3 show estimated accuracy age ranges (table 1) ascertained by this method for each of these samples. In addition to reducing age uncertainties for most flow units in the section, the data (fig. 3) indicate a one million year hiatus, between 25.2 and 24.2 Ma, and on that basis we refer herein to pre- and post-hiatus flows.

An approximate age scale (fig. 2) for the CRS was constructed using estimated age values. The As Sarat volcanics in the northern part of the field were erupted during a period of approximately 9 m.y. between 31 and 22 Ma. These data are comparable to K-Ar ages of 30 to 22 Ma for the equivalent Trap Series basalts directly to the south in the northern Yemen Arab Republic (Capaldi and others, 1983). In the CRS below the hiatus, the eruption rate decreases upward. Above the hiatus the eruption rate increases dramatically and most of the upper flows were erupted in a relatively short period of time between 24.2 and 23.5 Ma. The uppermost flow was erupted about 22.2 Ma.

**Table 1.**--Potassium-argon ages for volcanic rocks from the As Sarat volcanic field, Kingdom of Saudi Arabia.

| Field Number | Latitude N. | Longitude E. | Rock type | $K_2O$ wt. % | $^{40}Ar$ $10^{-11}$ mol/g | $^{40}Ar^{rad}$ % | Apparent age, m.y. ±1 sigma | Estimated Age Accuracy (m.y.) |
|---|---|---|---|---|---|---|---|---|
| 111779 | 18°09'27" | 43°09'58" | alkali basalt | 1.321 | 4.1656 | 25.4 | 21.8 ±1.3 | 20.5-23.1 |
| B-1 | do. | do. | do. | 1.315 | 4.30824 | 12.9 | 22.6 ±2.3 | 20.5-23.1 |
| 111780 | 18°09'34" | 43°09'55" | do. | 2.07 | 7.18045 | 46.7 | 23.9 ±0.7 | 23.2-24.2 |
| B-2 | 18°10'56" | 43°10'16" | hawaiite | 1.504 | 5.37982 | 50.7 | 24.7 ±0.7 | 24.0-24.2 |
| 112104 | do. | do. | do. | 1.59 | 5.70614 | 70.6 | 24.8 ±0.4 | -------- |
| 112105 | do. | 43°10'17" | do. | 1.443 | 5.81538 | 69.8 | 23.0 ±0.4 | -------- |
| B-3 | do. | 43°10'20" | do. | 1.576 | 5.04454 | 14.5 | 22.1 ±2.1 | 24.0-24.2 |
| 112108 | do. | 43°10'25" | alkali basalt | 0.885 | 3.30741 | 20.2 | 25.8 ±1.8 | 24.0-24.2 |
| B-4 | 18°10'55" | 43°10'40" | do. | 1.061 | 3.62366 | 51.8 | 23.6 ±0.6 | 24.0-24.2 |
| 112111 | do. | 43°10'41" | do. | 0.55 | 2.08867 | 24.0 | 26.2 ±1.6 | 25.2-27.7 |
| 112112 | 18°10'56" | 43°10'42" | do. | 0.396 | 1.45544 | 11.5 | 25.4 ±2.9 | 25.2-27.7 |
| 112113 | do. | 43°10'45" | basalt | 0.647 | 2.74638 | 27.8 | 29.3 ±1.6 | 27.7-30.1 |
| 112114 | 18°10'57" | 43°10'50" | do. | 0.39 | 0.882349 | 1.8 | 15.6 ±6.8 | -------- |
| 112115 | do. | 43°10'51" | do. | 0.28 | 1.11146 | 13.3 | 27.4 ±2.8 | 27.7-30.1 |
| 112118 | 18°10'58" | 43°10'52" | do. | 0.253 | 1.37174 | 27.9 | 37.3 ±2.0 | -------- |
| 112119 | do. | do. | do. | 0.268 | 0.686926 | 3.9 | 17.7 ±4.5 | -------- |
| 112120 | do. | 43°10'53" | do. | 0.234 | 1.01168 | 58.1 | 29.8 ±0.7 | 29.1-30.1 |
| 112120 | do. | do. | do. | 0.234 | 0.968654 | 24.3 | 28.5 ±1.7 | 29.1-30.1 |
| 112121 | do. | 43°10'54" | do. | 0.368 | 1.56358 | 51.3 | 29.3 ±0.8 | 29.1-30.1 |
| B-5 | 18°10'43" | 43°12'33" | do. | 0.298 | 1.3466 | 21.2 | 31.1 ±2.1 | 29.1-33.2 |
| AWB-1 | 18°09'25" | 43°06'52" | do. | 0.378 | 1.50521 | 31.0 | 27.5 ±1.3 | -------- |
| AW-2 | 18°09'25" | 43°04'41" | trachyte | 4.00 | 13.8664 | 73.5 | 23.9 ±0.4 | 23.5-24.3 |

Note: Uncertainties assigned to ages were determined using the curve of Tabor and others (1985). K-Ar ages were calculated using the constants for radioactive decay and abundance of $^{40}K$ recommended by the International Union of Geological Sciences Subcommission on Geochronolgy (Steiger and Jager, 1977). These constants are: $lambda_t = 0.581 \times 10^{-10}/yr$, $lambda_{beta} = 4.962 \times 10^{-10}/yr$, and $^{40}K/K_{total} = 1.167 \times 10^{-4}$ mol/mol.

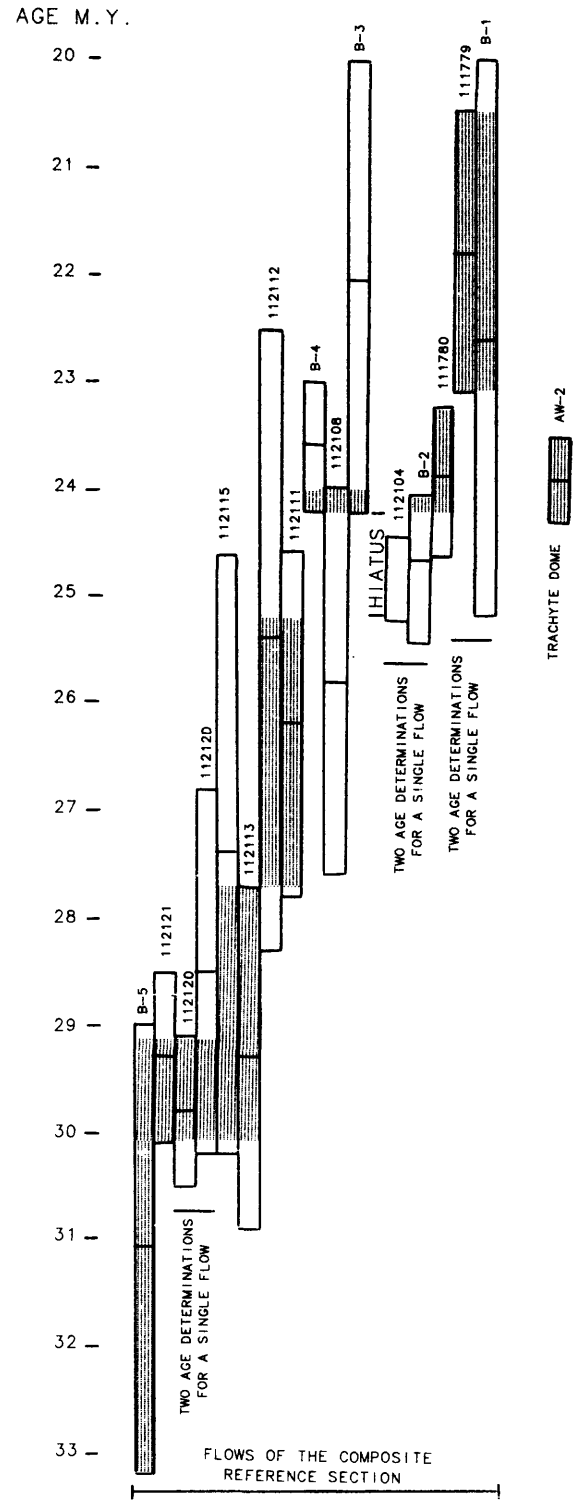


**Figure 3.**—Age evaluation diagram. Ages bars are plotted in order of decreasing stratigraphic age from left to right. Length of bar represents range of analytical uncertainty (one sigma); shaded area shows maximum uncertainty of the ages as indicated by stratigraphic relations.

# PETROGRAPHIC CHARACTERISTICS

Basalts of the As Sarat include intersertal, trachytic, and pilotaxitic textural types. Pre-hiatus flows are dominated by massive intersertal basalt, whereas post-hiatus flows are texturally trachytic and pilotaxitic basalt. Stratigraphic separation of the textural types is not complete as the three types are intercalated to a limited extent. Finely devitrified green glass, variably altered to clay minerals, forms trace to 22 percent of the basalts. All three textural types include spherical amygdules filled with calcite and a very fine-grained (unknown) green mineral. Olivine is present in all basalt samples and is partially altered to iddingsite or serpentine in most places. Pyroxene in the basalts is reddish- to purplish-brown, unaltered titaniferous clinopyroxene. Plagioclase crystals are unaltered and occur principally in the groundmass of As Sarat basalt, though it forms phenocrysts in a few of the pilotaxitic and trachytic basalts. Apatite and Fe-Ti oxides are the characteristic accessory minerals.

The intersertal basalt is distinctly coarser grained than either of the other two textural types; groundmass crystals range from 0.1 to 0.5 mm. Olivine (5 to 27 percent, mean 14) forms subhedral phenocrysts (0.15 percent, mean 5) in the intersertal basalt and is most abundant in this textural type. Clinopyroxene (21 to 41 percent, mean 31) is subophitic to ophitic. Groundmass plagioclase (22 to 52 percent, mean 38) forms euhedral to subhedral grains. Opaque oxides (1 and 12 percent, mean 7) are mostly magnetite but include some ilmenite. Glass (0 to 18 percent, mean 5) is interstitial.

The trachytic basalts are platy due to plagioclase lath alignment and have an average groundmass grain size of 0.1 to 0.2 mm. The pilotaxitic basalts are very fine grained, with average groundmass grain sizes of generally less than 0.1 mm. The trachytic and pilotaxitic basalts contain phenocrysts of olivine (1 to 14 percent, mean 7) and(or) plagioclase (37 to 60 percent, mean 45). Clinopyroxene (10 to 39 percent, mean 29) in the trachytic basalt is granular and very fine-grained. Opaque oxides (7 to 15 percent, mean 11) are mostly magnetite, although some of the trachytic basalts contain as much as or more ilmenite than magnetite. Glass (0 to 22 percent, mean 8) is interstitial.

Basalt dikes and necks of the As Sarat field are petrographically similar to the post-hiatus basalts. Some of the dikes and necks contain abundant clinopyroxene phenocrysts that may indicate crystal settling and accumulation in the magma chamber. Two of the basalt necks contained sparse small ($<2$ cm) peridotite (wehrlite) xenoliths and plagioclase xenocrysts.

The trachyte domes are composed of a leucocratic porphyry that contains about 30 percent carlsbad-twinned phenocrysts of anorthoclase 0.8 to 2.5 mm long in a trachytic groundmass. The groundmass is composed of feldspar, and minor opaque oxides and aegirine-augite, and has an average grain size of 0.1 mm. Small

quantities of feldspathoids are also present as phenocrysts and in the groundmass. Accessory minerals are biotite, arfvedsonite, opaque oxides, zircon, and apatite.

# CHEMICAL DATA

## Whole Rock

The alkaline/subalkaline classification of Irvine and Baragar (1971) was used to establish the alkalinity of As Sarat rocks (fig. 4), whereas, the classification system of the International Union of Geological Sciences (Le Bas and others, 1986) was used to determine rock names based on chemical compositions (fig. 4). Pre-hiatus flows in the CRS are composed, with two exceptions, of subalkaline basalt (average 3.02 percent $Na_2O + K_2O$ and 46.7 percent $SiO_2$, anhydrous). The post-hiatus flows include alkali basalt, hawaiite, and minor weakly alkaline basalt (average 4.52 percent $Na_2O + K_2O$ and 47.9 percent $SiO_2$, anhydrous). The intrusive trachytes are alkaline (average 11.36 percent $Na_2O + K_2O$ and 63.0 percent $SiO_2$, anhydrous) and the presence of alkali pyroboles indicates that they are peralkaline.

The As Sarat basalts are silica undersaturated. The majority of pre-hiatus basalts are hypersthene normative, whereas most of the post-hiatus basalts and all of the neck and dike samples are nepheline normative (as much as 9.8 percent). Compositions of dike and neck samples are similar to those of post-hiatus flows (figs. 4, 5; table 2). A distinctive feature of the As Sarat basalts is their unusually high $TiO_2$ contents. Average $TiO_2$ contents of the pre- and post-hiatus flow rocks, necks, and dikes are 1.92, 2.62, 2.63, and 2.94 anhydrous weight percent, respectively. The As Sarat rocks follow an AFM trend that is similar to that for Hawaiian alkaline basalts (fig. 6). The former have compositions very similar to those of the Termaber Formation of the Ethiopian Plateau (Mohr and Zanettin, 1989) but are somewhat more alkaline than the main Yemen Trap Series (Chiesa and others, 1989).

The abundances of the major oxides vary considerably between flows of the CRS (fig. 5); variation is most erratic for the pre-hiatus basalts. In post-hiatus basalts the average contents of $Al_2O_3$, $Na_2O$, $K_2O$, $TiO_2$, and $P_2O_5$, are distinctly greater, whereas total iron, MgO, CaO, and $Na_2O/K_2O$ are distinctly lower than in pre-hiatus subalkaline basalts of the CRS (table 2). A significant compositional discontinuity (fig. 5) is coincident with the eruption hiatus (between samples 112111 and 112110). Sample 112110 is compositionally transitional relative to pre- and post-hiatus basalt compositions. Its transitional character may indicate that initial (alkaline) lava erupted following the hiatus was contaminated by solidified, unerupted (subalkaline) lava remaining in eruption conduits at the end of pre-hiatus volcanism. In rocks of the As Sarat field, abundances of $Al_2O_3$, $Na_2O$, $K_2O$, $P_2O_5$, Ba, and Zr decrease with increasing MgO, whereas abundances of CaO, increase with increasing MgO; these variations are in accord with observed variation in mineral modes. Abundances of total iron, $TiO_2$, and MnO are uncorrelated with MgO variation.

Compositional data for each of the As Sarat field components (pre- and post-hiatus lava flows, necks, dikes, and trachyte domes) are characterized by groups of oxides and elements whose abundances display mutual covariation (table 3); correlation coefficients for abundances of oxides and elements within these groupings exceed 0.9. These covariance relations suggest that compositional variation within each component was controlled by a different mineral assemblage. Minerals inferred to have controlling influence on compositional variation occur as phenocryst phases. Fractional crystallization and partial melting, which can lead to removal, accumulation, and retention of crystals, result in predictable compositional variation because compositions of crystallizing/melting minerals are known or inferred. An additional consequence of fractional crystallization and partial melting is variable incompatible trace element enrichment of the liquid; an elemental covariation grouping, involving combinations of $K_2O$, $Na_2O$, Rb, Sr, Ba, Nb, Y, Zr, and Zn, denotes this process. Covariance relations among the rock groups indicates mineral component crystallization/crystal-settling control as follows:

**pre-hiatus basalts:** olivine, Fe-Ti oxides, apatite

**post-hiatus basalts:** clinopyroxene

**necks:** clinopyroxene, Fe-Ti oxides, apatite

**dikes:** clinopyroxene, Fe-Ti oxides

**trachytes:** plagioclase, aegirine, Fe-Ti oxides

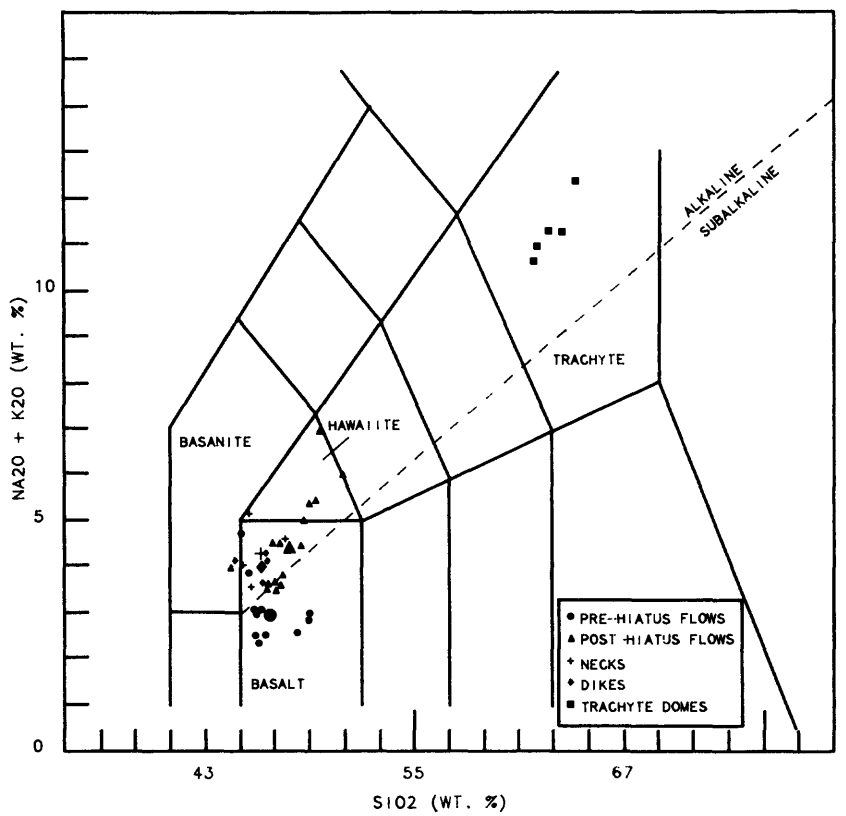


**Figure 4.**--Total alkalis-silica volcanic rock classification diagram after IUGS (Le Bas and others, 1986) showing compositions of samples from the As Sarat field (analyses recalculated to 100 percent anhydrous). Dashed line is the alkaline-subalkaline dividing line of Irvine and Baragar (1971). Enlarged plot symbols represent average compositions for rock type denoted by that symbol type.

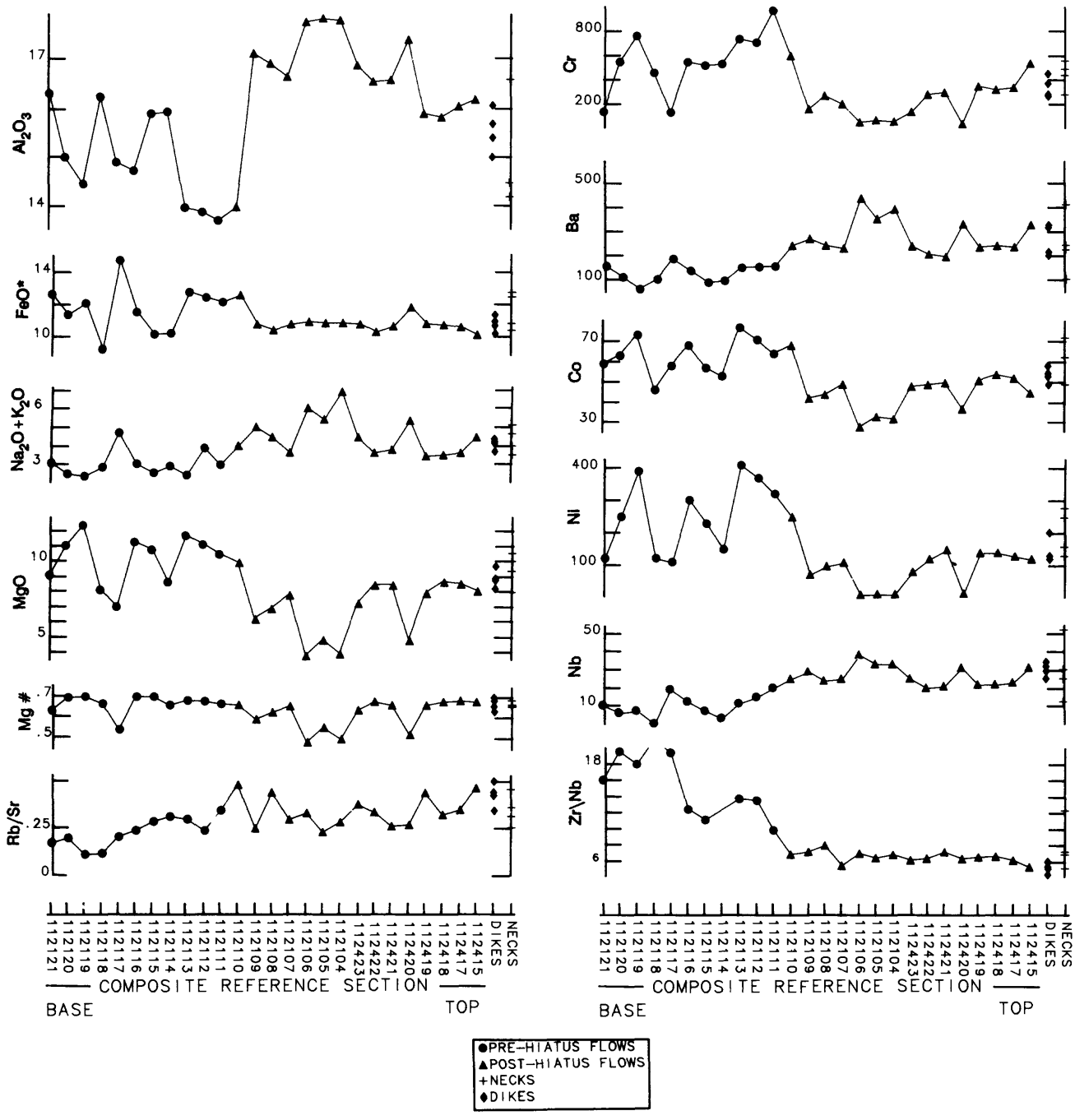


**Figure 5.**--Diagrams showing variations in major and trace element abundances versus stratigraphic position (analyses recalculated to 100 percent anhydrous). Data for major oxides expressed as weight percent; trace element data expressed in parts per million.

**Table 2.**--Major element, CIPW normative (calculated for analyses normalized to 100 percent, anhydrous) and trace element compositions for samples of the As Sarat field, Kingdom of Saudi Arabia.

| | Flows | | | | | | | | | | | | | |
|---|---|---|---|---|---|---|---|---|---|---|---|---|---|---|
| Field No. | 112121 | 112120 | 112119 | 112118 | 112117 | 112116 | 112115 | 112114 | 112113 | 112112 | 112111 | 112110 | 112109 | 112108 |
| Latitude: ($18^{o}$N.) | 10'58" | 10'58" | 10'58" | 10'58" | 10'58" | 10'57" | 10'57" | 10'57" | 10'56" | 10'56" | 10'55" | 10'55" | 10'56" | 10'56" |
| Longitude: ($43^{o}$E.) | 10'54" | 10'53" | 10'53" | 10'52" | 10'52" | 10'51" | 10'51" | 10'48" | 10'45" | 10'42" | 10'41" | 10'40" | 10'32" | 10'25" |
| | Chemical analyses, weight percent | | | | | | | | | | | | | |
| $SiO_2$ | 43.9 | 43.7 | 45.0 | 48.0 | 43.9 | 44.5 | 46.6 | 46.5 | 43.1 | 45.1 | 44.0 | 43.3 | 47.6 | 47.4 |
| $Al_2O_3$ | 15.6 | 14.1 | 14.1 | 15.9 | 14.5 | 14.2 | 15.3 | 15.1 | 13.1 | 13.7 | 13.1 | 13.6 | 16.7 | 16.5 |
| $Fe_2O_3$ | 3.56 | 3.54 | 3.64 | 4.49 | 6.36 | 6.90 | 4.18 | 7.31 | 8.67 | 5.78 | 7.54 | 8.03 | 4.40 | 4.97 |
| FeO | 9.30 | 7.97 | 8.96 | 5.50 | 9.12 | 5.40 | 6.50 | 3.59 | 4.62 | 7.58 | 5.27 | 5.46 | 7.02 | 6.15 |
| MgO | 8.70 | 10.4 | 12.1 | 7.94 | 6.79 | 10.9 | 10.4 | 8.17 | 11.0 | 11.0 | 10.0 | 9.66 | 6.09 | 6.73 |
| CaO | 8.89 | 9.81 | 9.48 | 12.1 | 7.98 | 9.68 | 9.79 | 10.3 | 9.09 | 9.53 | 11.0 | 10.6 | 7.97 | 8.81 |
| $Na_2O$ | 2.40 | 1.92 | 2.05 | 2.54 | 3.82 | 2.48 | 2.21 | 2.47 | 1.70 | 3.22 | 2.29 | 2.83 | 3.87 | 3.40 |
| $K_2O$ | 0.53 | 0.43 | 0.25 | 0.25 | 0.78 | 0.43 | 0.26 | 0.29 | 0.57 | 0.58 | 0.55 | 1.03 | 0.99 | 0.95 |
| $TiO_2$ | 2.26 | 1.74 | 1.67 | 1.13 | 3.33 | 1.89 | 1.03 | 1.27 | 2.01 | 2.11 | 1.88 | 2.59 | 2.30 | 2.18 |
| $P_2O_5$ | .37 | .27 | .20 | .15 | .71 | .30 | .16 | .18 | .26 | .39 | .33 | 0.41 | .61 | .50 |
| MnO | .18 | .17 | .18 | .16 | .19 | .17 | .18 | .18 | .20 | .19 | .19 | .19 | .18 | .17 |
| $H_2O^1$ | 3.47 | 5.66 | 2.31 | 1.66 | 3.10 | 3.42 | 3.09 | 4.39 | 6.53 | 1.48 | 4.16 | 2.36 | 1.84 | 2.25 |
| Total | 99.16 | 99.71 | 99.94 | 99.82 | 100.58 | 100.27 | 99.70 | 99.75 | 100.85 | 100.66 | 100.13 | 100.06 | 99.57 | 100.01 |
| | CIPW norms, weight percent | | | | | | | | | | | | | |
| Q | - | - | - | - | - | - | - | - | - | - | - | - | - | - |
| or | 3.3 | 2.7 | 1.5 | 1.5 | 4.8 | 2.6 | 1.6 | 1.8 | 3.6 | 3.5 | 3.4 | 6.3 | 6.0 | 5.8 |
| ab | 21.3 | 17.3 | 17.8 | 22.0 | 24.4 | 19.7 | 19.4 | 22.1 | 15.4 | 17.3 | 15.5 | 10.3 | 32.3 | 29.4 |
| an | 31.7 | 30.5 | 29.3 | 31.9 | 20.7 | 27.4 | 32.3 | 30.9 | 28.2 | 21.5 | 25.0 | 22.0 | 25.9 | 27.7 |
| ne | - | - | - | - | 4.8 | 1.2 | - | - | - | 5.6 | 2.6 | 7.8 | .7 | .1 |
| di | 9.8 | 15.8 | 14.3 | 23.2 | 12.7 | 16.6 | 13.9 | 17.8 | 14.8 | 19.4 | 24.4 | 24.0 | 8.7 | 11.4 |
| hy | 3.9 | 5.8 | 5.3 | 3.1 | - | - | 11.1 | 9.4 | 8.6 | - | - | - | - | - |
| ol | 22.6 | 21.8 | 26.0 | 14.1 | 21.9 | 26.2 | 17.6 | 13.4 | 22.6 | 25.7 | 22.6 | 21.5 | 18.6 | 18.5 |
| mt | 2.1 | 1.9 | 2.0 | 1.6 | 2.5 | 1.9 | 1.7 | 1.7 | 2.1 | 2.1 | 2.0 | 2.1 | 1.8 | 1.8 |
| il | 4.5 | 3.5 | 3.3 | 2.2 | 6.5 | 3.7 | 2.0 | 2.6 | 4.1 | 4.1 | 3.7 | 5.1 | 4.5 | 4.3 |
| ap | 0.9 | 0.7 | 0.5 | 0.4 | 1.7 | .7 | 0.4 | 0.5 | 0.7 | 0.9 | 0.8 | 1.0 | 1.5 | 1.2 |
| | Trace elements, parts per million | | | | | | | | | | | | | |
| Rb | 12 | 15 | 4 | 4 | 21 | 12 | 8 | 10 | 14 | 14 | 20 | 30 | 15 | 24 |
| Sr | 713 | 763 | 362 | 338 | 1042 | 512 | 279 | 321 | 470 | 595 | 575 | 621 | 604 | 543 |
| Y | 22 | 20 | 20 | 21 | 20 | 20 | 23 | 22 | 19 | 24 | 21 | 21 | 27 | 25 |
| Zr | 160 | 117 | 126 | 71 | 369 | 149 | 78 | 91 | 151 | 202 | 196 | 172 | 208 | 190 |
| Nb | 10 | 6 | 7 | <3 | 19 | 12 | 7 | 3 | 11 | 15 | 20 | 25 | 29 | 24 |
| Ba | 156 | 111 | 62 | 102 | 187 | 138 | 90 | 94 | 151 | 152 | 156 | 242 | 269 | 242 |
| Co | 59 | 63 | 73 | 46 | 58 | 68 | 57 | 53 | 77 | 71 | 64 | 68 | 42 | 44 |
| Cr | 140 | 550 | 760 | 460 | 130 | 550 | 520 | 530 | 740 | 710 | 970 | 600 | 160 | 270 |
| Cu | 68 | 58 | 89 | 60 | 61 | 100 | 86 | 54 | 79 | 79 | 69 | 81 | 49 | 45 |
| Ni | 120 | 250 | 390 | 120 | 110 | 300 | 230 | 150 | 410 | 370 | 320 | 250 | 72 | 96 |
| Sc | 27 | 30 | 30 | 40 | 10 | 27 | 33 | 34 | 24 | 24 | 27 | 23 | 20 | 23 |
| V | 210 | 220 | 240 | 250 | 200 | 230 | 220 | 250 | 240 | 240 | 220 | 260 | 150 | 170 |
| Zn | 88 | 79 | 83 | 61 | 120 | 75 | 67 | 73 | 88 | 97 | 96 | 97 | 70 | 72 |

**Table 2.--Major element, CIPW normative (continued)**

| | Flows | | | | | | | | | | | | | |
|---|---|---|---|---|---|---|---|---|---|---|---|---|---|---|
| Field No. | 112107 | 112106 | 112105 | 112104 | 112423 | 112422 | 112421 | 112420 | 112419 | 112418 | 112417 | 112415 | 112101 | 112102 |
| Latitude: ($18^{o}$N.) | 10'56" | 10'56" | 10'56" | 10'56" | 09'40" | 09'39" | 09'37" | 09'35" | 09'33" | 09'31" | 09'29" | 09'27" | 55'44"[2] | 55'46"[2] |
| Longitude: ($43^{o}$E.) | 10'20" | 10'19" | 10'17" | 10'16" | 09'53" | 09'53" | 09'54" | 09'54" | 09'55" | 09'56" | 09'57" | 09'58" | 15'26" | 15'51" |
| | Chemical analyses, weight percent | | | | | | | | | | | | | |
| $SiO_2$ | 45.8 | 49.0 | 48.3 | 49.1 | 46.2 | 46.5 | 46.4 | 47.7 | 45.7 | 45.2 | 44.7 | 46.7 | 44.7 | 50.3 |
| $Al_2O_3$ | 16.2 | 17.1 | 17.4 | 17.6 | 16.6 | 16.2 | 16.2 | 16.9 | 15.4 | 15.3 | 15.3 | 15.9 | 14.1 | 17.4 |
| $Fe_2O_3$ | 5.11 | 6.14 | 5.04 | 5.18 | 4.32 | 3.88 | 3.54 | 5.71 | 6.65 | 5.53 | 4.79 | 4.07 | 2.98 | 4.97 |
| FeO | 6.38 | 5.45 | 6.53 | 6.50 | 7.18 | 7.04 | 7.70 | 6.83 | 4.90 | 5.82 | 6.22 | 6.78 | 9.74 | 6.24 |
| MgO | 7.58 | 3.67 | 4.70 | 3.92 | 7.19 | 8.31 | 8.29 | 4.71 | 7.72 | 8.39 | 8.17 | 7.99 | 9.48 | 3.73 |
| CaO | 9.77 | 5.90 | 6.47 | 6.12 | 9.38 | 10.00 | 9.07 | 6.54 | 10.3 | 10.2 | 9.98 | 9.49 | 9.96 | 6.93 |
| $Na_2O$ | 2.63 | 4.22 | 4.03 | 5.35 | 3.38 | 2.70 | 2.91 | 4.03 | 2.40 | 2.49 | 2.52 | 3.16 | 3.15 | 4.26 |
| $K_2O$ | 0.92 | 1.59 | 1.28 | 1.52 | 1.03 | 0.83 | 0.82 | 1.19 | 0.95 | 0.92 | 0.91 | 1.26 | 1.25 | 1.84 |
| $TiO_2$ | 2.56 | 2.58 | 3.20 | 2.87 | 2.62 | 2.17 | 2.26 | 2.92 | 2.59 | 2.52 | 2.47 | 2.44 | 2.84 | 2.20 |
| $P_2O_5$ | .33 | 0.67 | 0.55 | 0.66 | 0.37 | .31 | .37 | .66 | .36 | .36 | .35 | 0.56 | 0.56 | 0.93 |
| MnO | .17 | .17 | .16 | .17 | .17 | .17 | .18 | .19 | .17 | .18 | .16 | .17 | .21 | .22 |
| $H_2O^1$ | 2.80 | 2.92 | 2.75 | .66 | 1.10 | 1.71 | 1.47 | 2.31 | 3.32 | 3.25 | 2.26 | 1.03 | .71 | 2.07 |
| Total | 100.25 | 99.41 | 100.41 | 99.57 | 99.54 | 99.82 | 99.21 | 99.69 | 100.46 | 100.16 | 97.83 | 99.55 | 99.68 | 101.09 |
| | CIPW norms, weight percent | | | | | | | | | | | | | |
| Q | - | - | - | - | - | - | - | - | - | - | - | - | - | - |
| or | 5.6 | 9.8 | 7.8 | 9.1 | 6.2 | 5.0 | 5.0 | 7.3 | 5.8 | 5.6 | 5.7 | 7.6 | 7.5 | 11.0 |
| ab | 22.9 | 37.2 | 35.1 | 36.5 | 22.5 | 22.9 | 25.3 | 35.2 | 21.0 | 20.4 | 20.8 | 22.5 | 13.8 | 36.5 |
| an | 30.6 | 24.0 | 26.3 | 19.8 | 27.6 | 30.3 | 29.5 | 25.3 | 29.4 | 28.9 | 29.1 | 25.9 | 20.9 | 23.2 |
| ne | - | - | - | 5.1 | 3.6 | .2 | - | - | - | .8 | .9 | 2.6 | 7.1 | - |
| di | 14.0 | 1.6 | 2.5 | 5.5 | 14.2 | 15.0 | 11.6 | 3.1 | 17.2 | 17.2 | 16.7 | 14.9 | 20.7 | 4.6 |
| hy | .5 | 8.4 | 6.5 | - | - | - | .7 | 4.8 | 2.0 | - | - | - | - | 3.9 |
| ol | 18.8 | 10.4 | 12.5 | 15.1 | 18.1 | 19.9 | 21.0 | 15.1 | 16.8 | 19.5 | 19.3 | 18.8 | 21.2 | 12.6 |
| mt | 1.8 | 1.8 | 1.8 | 1.8 | 1.8 | 1.7 | 1.8 | 2.0 | 1.8 | 1.8 | 1.8 | 1.7 | 2.0 | 1.8 |
| il | 5.0 | 5.1 | 6.3 | 5.5 | 5.1 | 4.2 | 4.4 | 5.7 | 5.1 | 5.0 | 4.9 | 4.7 | 5.5 | 4.2 |
| ap | 0.8 | 1.7 | 1.3 | 1.6 | 0.9 | 0.8 | 0.9 | 1.6 | 0.9 | 0.9 | 0.9 | 1.4 | 1.3 | 2.2 |
| | Trace elements, parts per million | | | | | | | | | | | | | |
| Rb | 15 | 28 | 20 | 25 | 19 | 16 | 16 | 20 | 26 | 22 | 21 | 29 | 30 | 40 |
| Sr | 503 | 840 | 876 | 884 | 497 | 471 | 602 | 736 | 592 | 670 | 598 | 617 | 734 | 1222 |
| Y | 22 | 25 | 25 | 28 | 27 | 22 | 22 | 26 | 20 | 19 | 23 | 23 | 25 | 25 |
| Zr | 138 | 265 | 213 | 226 | 154 | 128 | 151 | 198 | 145 | 146 | 142 | 166 | 201 | 253 |
| Nb | 25 | 38 | 33 | 33 | 25 | 20 | 21 | 31 | 22 | 22 | 23 | 31 | 39 | 52 |
| Ba | 229 | 435 | 352 | 390 | 237 | 205 | 195 | 328 | 236 | 240 | 235 | 326 | 297 | 581 |
| Co | 49 | 28 | 33 | 32 | 48 | 49 | 50 | 37 | 51 | 54 | 52 | 45 | 56 | 21 |
| Cr | 200 | 49 | 67 | 59 | 140 | 280 | 300 | 41 | 350 | 320 | 340 | 540 | 640 | <1 |
| Cu | 59 | 26 | 30 | 24 | 61 | 71 | 59 | 26 | 67 | 69 | 63 | 49 | 64 | 12 |
| Ni | 110 | 10 | 11 | 11 | 81 | 120 | 150 | 14 | 140 | 140 | 130 | 120 | 190 | <2 |
| Sc | 26 | 7 | 10 | 10 | 25 | 28 | 22 | 14 | 25 | 26 | 26 | 23 | 25 | 5 |
| V | 200 | 67 | 98 | 74 | 190 | 200 | 190 | 140 | 230 | 230 | 220 | 190 | 210 | 85 |
| Zn | 71 | 70 | 56 | 66 | 71 | 68 | 68 | 66 | 77 | 70 | 74 | 69 | 85 | 87 |

**Table 2.--Major element, CIPW normative (continued)**

| | Necks | | | | Dikes | | | | Trachyte domes | | | | |
|---|---|---|---|---|---|---|---|---|---|---|---|---|---|
| Field No. | 112052 | 112054 | 112087 | 112103 | 112092 | 112094 | 112097 | 112098 | 108557 | 108894 | 108896 | 108897 | 108899 |
| Latitude: (18°N.) | 02'14" | 09'28" | 00'11" | 00'06" | 00'27" | 59'43"[2] | 02'34" | 02'01" | 07'40" | 07'23" | 07'34" | 09'22" | 08'24" |
| Longitude: (43°E.) | 21'40" | 19'50" | 33'01" | 17'21" | 11'23" | 10'31" | 10'29" | 10'26" | 07'17" | 08'40" | 08'23" | 04'43" | 06'30" |
| | | | | | Chemical analyses, weight percent | | | | | | | | |
| $SiO_2$ | 45.1 | 45.0 | 45.2 | 46.9 | 45.6 | 45.8 | 45.3 | 44.1 | 63.2 | 59.5 | 58.8 | 61.3 | 60.8 |
| $Al_2O_3$ | 14.3 | 14.1 | 14.3 | 16.3 | 15.1 | 15.7 | 15.2 | 14.7 | 17.6 | 17.6 | 17.3 | 17.5 | 17.9 |
| $Fe_2O_3$ | 3.33 | 3.6 | 4.06 | 4.99 | 3.86 | 3.56 | 3.43 | 2.49 | 2.48 | 1.99 | 3.52 | 2.72 | 2.10 |
| FeO | 7.71 | 9.58 | 9.39 | 6.58 | 7.68 | 7.68 | 7.26 | 9.37 | 1.50 | 3.27 | 2.08 | 1.84 | 2.75 |
| MgO | 9.24 | 10.0 | 10.4 | 7.86 | 9.54 | 8.06 | 8.69 | 8.68 | 0.17 | 0.51 | 0.64 | 0.39 | 0.46 |
| CaO | 10.4 | 9.86 | 9.32 | 8.35 | 9.77 | 9.73 | 9.60 | 10.8 | .85 | 1.74 | 1.88 | 1.32 | 1.37 |
| $Na_2O$ | 3.40 | 2.84 | 2.85 | 3.54 | 2.65 | 2.80 | 2.78 | 2.72 | 7.44 | 6.56 | 6.19 | 6.61 | 6.62 |
| $K_2O$ | 1.69 | 1.15 | 0.63 | 1.00 | 0.96 | 1.28 | 1.43 | 1.38 | 4.73 | 3.97 | 3.92 | 4.31 | 4.37 |
| $TiO_2$ | 2.99 | 2.74 | 2.27 | 2.39 | 2.55 | 2.71 | 2.90 | 3.37 | .05 | .22 | .21 | .14 | .17 |
| $P_2O_5$ | .64 | 0.49 | .35 | 0.46 | .37 | 0.56 | 0.36 | 0.47 | .05 | .18 | .19 | .11 | .11 |
| MnO | .20 | .20 | .18 | .17 | .17 | .17 | .16 | .17 | .21 | .20 | .20 | .20 | .17 |
| $H_2O^1$ | .86 | .50 | .29 | 1.02 | 1.88 | 1.88 | 1.95 | .70 | 1.05 | 3.88 | 4.44 | 3.15 | 2.57 |
| Total | 99.86 | 100.11 | 99.24 | 99.56 | 100.13 | 99.93 | 99.06 | 98.95 | 99.33 | 99.62 | 99.37 | 99.59 | 99.39 |
| | | | | | CIPW norms, weight percent | | | | | | | | |
| Q | - | - | - | - | - | - | - | - | - | - | - | .3 | - |
| or | 10.1 | 6.8 | 3.8 | 6.0 | 5.8 | 7.7 | 8.7 | 8.3 | 28.5 | 24.5 | 24.5 | 26.5 | 26.7 |
| ab | 11.1 | 14.9 | 19.4 | 26.8 | 19.7 | 20.6 | 18.0 | 11.6 | 61.9 | 58.1 | 55.3 | 58.1 | 58.0 |
| an | 19.0 | 22.5 | 24.7 | 26.1 | 27.0 | 27.1 | 25.6 | 24.3 | .7 | 7.2 | 8.3 | 5.6 | 6.3 |
| ne | 9.8 | 5.0 | 2.7 | 2.0 | 1.8 | 2.0 | 3.4 | 6.4 | 1.2 | - | - | - | - |
| di | 23.5 | 19.2 | 16.2 | 10.7 | 16.2 | 15.1 | 17.2 | 22.1 | 2.9 | .6 | 0.2 | 0.4 | - |
| hy | - | - | - | - | - | - | - | - | - | 3.6 | 8.8 | 7.9 | 4.1 |
| ol | 17.5 | 23.1 | 25.9 | 20.9 | 21.9 | 19.1 | 18.9 | 17.7 | 4.0 | 4.4 | 1.1 | - | 3.5 |
| mt | 1.8 | 2.1 | 2.1 | 1.8 | 1.8 | 1.8 | 1.7 | 1.9 | .6 | .9 | .9 | .7 | .8 |
| il | 5.8 | 5.2 | 4.4 | 4.6 | 4.9 | 5.3 | 5.7 | 6.5 | .1 | .4 | .4 | .3 | .3 |
| ap | 1.5 | 1.2 | 0.8 | 1.1 | .9 | 1.4 | 0.9 | 1.1 | .1 | .5 | .5 | .3 | .3 |
| | | | | | Trace elements, parts per million | | | | | | | | |
| Rb | 32 | 31 | 13 | 22 | 21 | 33 | 25 | 25 | 165 | 103 | 111 | 118 | 106 |
| Sr | 882 | 675 | 502 | 692 | 490 | 646 | 560 | 717 | 91 | 284 | 301 | 128 | 189 |
| Y | 24 | 26 | 24 | 24 | 26 | 22 | 24 | 24 | 41 | 29 | 28 | 29 | 26 |
| Zr | 272 | 217 | 148 | 173 | 151 | 185 | 151 | 140 | 937 | 656 | 609 | 758 | 645 |
| Nb | 52 | 30 | 12 | 25 | 25 | 34 | 29 | 32 | 146 | 103 | 111 | 107 | 93 |
| Ba | 413 | 226 | 103 | 344 | 216 | 321 | 316 | 327 | 196 | 885 | 868 | 723 | 623 |
| Co | 49 | 62 | 72 | 49 | 58 | 49 | 55 | 53 | <1 | 2 | 3 | <1 | 2 |
| Cr | 490 | 560 | 440 | 280 | 450 | 280 | 270 | 370 | <1 | <1 | <1 | <1 | <1 |
| Cu | 59 | 77 | 87 | 37 | 77 | 69 | 58 | 61 | 7 | 7 | 6 | 7 | 6 |
| Ni | 170 | 260 | 290 | 140 | 20 | 120 | 120 | 130 | <2 | <2 | <2 | <2 | <2 |
| Sc | 24 | 26 | 23 | 20 | 27 | 22 | 25 | 25 | <2 | <2 | <2 | <2 | <2 |
| V | 240 | 220 | 250 | 160 | 220 | 220 | 240 | 250 | <2 | <2 | 2 | <2 | <2 |
| Zn | 92 | 99 | 110 | 83 | 85 | 84 | 72 | 80 | 140 | 95 | 110 | 110 | 100 |

**Table 2.--Major element, CIPW normative (continued)**

| | AS SARAT AVERAGES | | | | | MORB[3] | Lith[4] | Rahat[5] |
|---|---|---|---|---|---|---|---|---|
| | CRS flows | Subalka-line flows | Alkaline flows | Necks | Dikes | Trachyte Domes | | | |
| | Chemical analyses, weight percent | | | | | | | | |
| $SiO_2$ | 45.92 | 44.94 | 46.64 | 45.55 | 45.20 | 60.72 | 49.34 | 46.68 | 47.12 |
| $Al_2O_3$ | 15.45 | 14.43 | 16.19 | 14.75 | 15.18 | 17.58 | 17.04 | 15.41 | 16.08 |
| $Fe_2O_3$ | 3.74 | 3.33 | 4.04 | 3.66 | 3.34 | 1.66 | 1.99 | 4.30 | - |
| FeO | 7.99 | 8.78 | 7.41 | 8.25 | 8.00 | 3.10 | 6.82 | 6.18 | 11.85 |
| MgO | 8.10 | 9.76 | 6.87 | 9.38 | 8.74 | 0.43 | 7.19 | 7.28 | 7.67 |
| CaO | 9.16 | 9.79 | 8.71 | 9.48 | 9.98 | 1.43 | 11.72 | 9.68 | 9.78 |
| $Na_2O$ | 2.96 | 2.46 | 3.33 | 3.16 | 2.74 | 6.68 | 2.73 | 3.17 | 3.59 |
| $K_2O$ | 0.81 | 0.45 | 1.08 | 1.12 | 1.26 | 4.26 | 0.16 | 0.86 | 0.80 |
| $TiO_2$ | 2.25 | 1.85 | 2.55 | 2.60 | 2.88 | 0.16 | 1.49 | 1.86 | 2.48 |
| $P_2O_5$ | 0.40 | 0.30 | 0.47 | 0.48 | 0.44 | 0.13 | .16 | .35 | .50 |
| MnO | 0.18 | 0.18 | 0.17 | 0.19 | 0.17 | 0.20 | .17 | .17 | .19 |
| $H_2O$[1] | 2.74 | 3.57 | 2.14 | 0.67 | 1.60 | 3.02 | 1.17 | 2.37 | .45 |
| Total | 99.70 | 99.84 | 99.60 | 99.66 | 99.52 | 99.37 | 99.98 | 98.31 | 100.06 |
| | CIPW norms, weight percent | | | | | | | | |
| or | 5.0 | 2.8 | 6.6 | 6.7 | 7.6 | 26.2 | 1.0 | 5.3 | 4.7 |
| ab | 24.9 | 21.7 | 27.2 | 18.4 | 17.4 | 58.8 | 23.4 | 25.9 | 23.2 |
| an | 27.4 | 28.1 | 26.8 | 23.2 | 26.0 | 5.6 | 34.2 | 26.4 | 25.4 |
| ne | .5 | - | 1.0 | 4.8 | 3.4 | - | - | 1.2 | 3.9 |
| di | 13.8 | 16.6 | 11.9 | 17.5 | 17.7 | .8 | 14.5 | 17.5 | 16.3 |
| hy | - | .2 | - | - | - | 4.2 | 7.1 | - | - |
| ol | 21.1 | 24.3 | 18.7 | 21.5 | 19.4 | 3.1 | 2.5 | 17.5 | 18.9 |
| mt | 1.9 | 2.0 | 1.8 | 1.9 | 1.8 | .8 | 2.9 | 1.7 | 1.9 |
| il | 4.4 | 3.7 | 5.0 | 5.0 | 5.6 | .3 | 2.9 | 3.4 | 4.7 |
| ap | 1.0 | .7 | 1.2 | 1.2 | 1.1 | .3 | 0.4 | 0.9 | 1.2 |
| | Trace elements, parts per million | | | | | | | | |
| Rb | 18 | 12 | 22 | 25 | 26 | 128 | 1.16 | 22 | 7 |
| Sr | 601 | 543 | 644 | 688 | 603 | 173 | 40 | 424 | 550 |
| Y | 23 | 21 | 24 | 25 | 24 | 27 | 43 | - | 25 |
| Zr | 167 | 156 | 176 | 203 | 157 | 675 | 95 | 151 | 197 |
| Nb | 20 | 10 | 27 | 30 | 30 | 110 | <30 | - | 23 |
| Ba | 214 | 127 | 277 | 247 | 295 | 716 | 7.8 | - | 108 |
| Co | 52 | 63 | 46 | 58 | 54 | 2 | 32 | - | - |
| Cr | 376 | 551 | 248 | 443 | 343 | 1 | 297 | 180 | 215 |
| Cu | 61 | 73 | 52 | 65 | 66 | 7 | 77 | - | 72 |
| Ni | 163 | 252 | 97 | 215 | 143 | 2 | 97 | - | 122 |
| Sc | 24 | 28 | 21 | 23 | 25 | 2 | 61 | - | 23 |
| V | 197 | 229 | 174 | 218 | 233 | 2 | 292 | - | 228 |
| Zn | 76 | 84 | 71 | 96 | 80 | 111 | - | - | 86 |

1 $H_2O$ is loss on ignition
2 Latitude is prefixed by $17^o$
3 Mid ocean ridge basalt (Engel and others, 1965; Hart, 1971)
4 Average of 8 Red Sea basalts (sample numbers 165006, 165582, 165567, 165661, 165881, 175834, 165767, and 175771) from the central Arabian coastal plain (Pallister, 1987)
5 Average of 64 alkali olivine basalts from Harrat Rahat (Camp and Roobol, 1989)

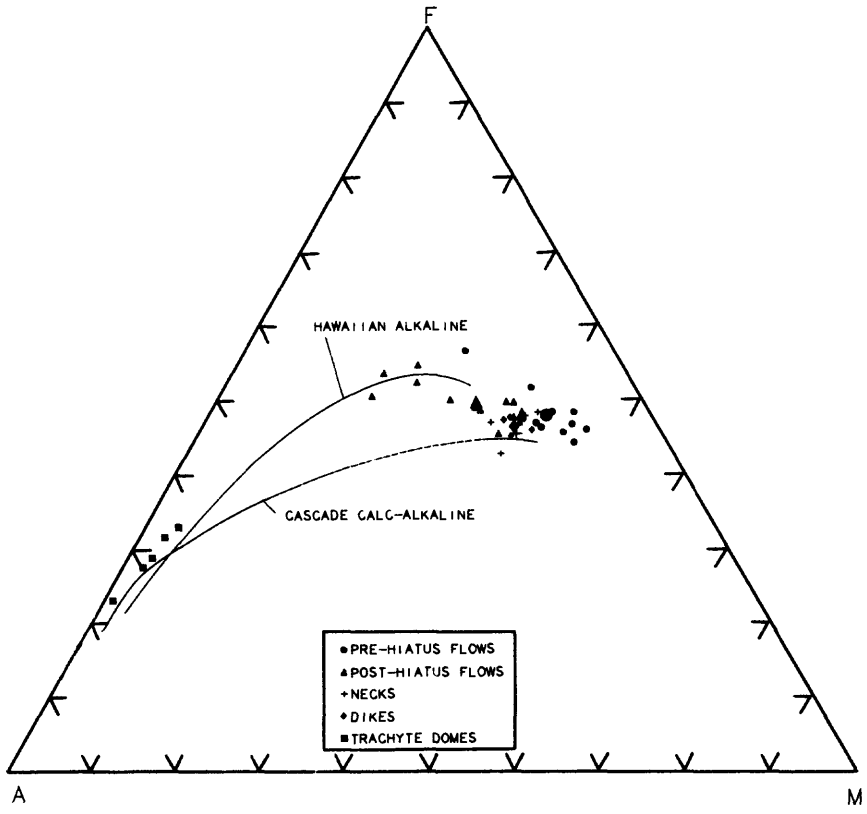


**Figure 6.**--Ternary AFM diagram showing compositions of samples from the As Sarat field. Enlarged plot symbols represent average compositions for rock type denoted by that symbol type. Trend lines from Irvine and Baragar (1971).

**Table 3.**--Groupings, by lithology, whose constituent oxide and elemental pairs display abundance covariation in components of the As Sarat field. Most oxide/element pairs within a grouping have correlation coefficients $\geq 0.9$.

| Lithology | Oxide/element groupings | Inferred controlling phases |
|---|---|---|
| Pre-hiatus basalt | $FeO+TiO_2+P_2O_5+Zr+Sr+Zn+Co$ | iron-titanium oxide and apatite |
| | $MgO+Ni+Cr$ | olivine |
| | $K_2O+Rb+Ba+Zn$ | melt incompatible trace element enrichment |
| Post-hiatus basalt | $CaO+MgO+Co+Cu+Ni+Sc+V$ | Ca/Mg-clinopyroxene |
| | $K_2O+Ba+Nb+Zr+P_2O_5$ | melt incompatible trace element enrichment and apatite |
| Basalt necks | $MgO+FeO+Co+Cu+Ni+Zn+Nb+Sc$ | Mg/Fe-clinopyroxene |
| | $CaO+MnO+Cr+Sc$ | unknown |
| | $K_2O+TiO_2+P_2O_5+Sr+Ba+Zr+Rb+Nb$ | melt incompatible trace element enrichment, apatite, and iron-titanium oxide |
| Basalt dikes | $MgO+Co+Sc+Y+Cu+Ni+V$ | Mg-clinopyroxene |
| | $K_2O+Ba$ | melt incompatible trace element enrichment |
| | $Ti_2O+V$ | iron-titanium oxide |
| Trachyte domes | $SiO_2+K_2O+Na_2O+Zr+Y+Zn+Nb$ | melt incompatible trace element enrichment |
| | $FeO+MgO-CaO+TiO_2+P_2O_5+Sr+Ba+Ca$ | aegirine and apatite |

The abundances of the trace elements also vary considerably within the flows of the CRS (fig. 5); variation is about equally erratic, over similar ranges, in pre- and post-hiatus basalts. In the post-hiatus basalts the average contents of Rb, Sr, Ba, Zr, and Nb are distinctly greater, whereas those of Co, Cr, Cu, Ni, Sc, V, and Zn are distinctly lower than in the pre-hiatus flows of the CRS (table 2). The previously described compositional discontinuity coincident with the hiatus is also denoted by trace element abundances; sample 112110 is similarly compositionally transitional. In rocks of the As Sarat field abundances of Co, Cu, Ni, Sc, V, Zn, and Cr, increase with increasing MgO, whereas abundances of Ba, Y, Nb, Rb, Zr, and Sr decrease with increasing MgO. Ternary proportions of Ti, Zr, and Y (fig. 7) in As Sarat basalt are similar to those characteristic of within-plate basalts; three of the pre-hiatus basalts have compositions similar to that of ocean floor basalt.

Total REE contents and chondrite-normalized REE patterns for selected samples of the CRS are strikingly similar (table 4, fig. 8). Individual patterns show slight light-REE (LREE) enrichment and very small positive Eu anomalies. Post-hiatus basalts are more LREE enriched ($La/Lu_{CN} = 6.36$ versus 3.50) than average pre-hiatus basalt. Chondrite normalized patterns and REE contents for one basalt neck and one basalt dike are essentially indistinguishable from those of the pre- and post-hiatus flow rocks, respectively. However, the trachyte contains a much greater total-REE content and its chondrite normalized REE pattern shows strong LREE enrichment and moderate heavy REE (HREE) enrichment centered on a moderate negative europium anomaly. REE contents of the As Sarat basalts are similar to those reported for alkali basalts by Camp and Roobol (1989) for Miocene to Recent flows of Harrat Rahat (600 km to the north-northwest) and by Pallister (1987) for Tertiary flows and dikes of the Red Sea coastal plain (400 km to the northwest).

Spidergrams (fig. 9) facilitate comparison of incompatible trace element abundances in the As Sarat basalts with those in other continental alkali basalts. With the exception of weakly positive Sr and P anomalies in the pre- and post-hiatus basalts, respectively, and moderate negative Ba and Th anomalies in all components of the As Sarat field, spidergrams for the As Sarat basalts are relatively smooth and gently negatively sloping. Abundances of the incompatible trace elements are greater in the post-hiatus basalts than in the pre-hiatus basalts; in particular the post-hiatus basalts are more notably enriched in the most incompatible trace elements. Basalt necks and dikes of the As Sarat field are characterized by spidergrams that are most similar to those of the pre- and post-hiatus basalts, respectively. Positive Nb anomalies characteristic of many continental alkali basalts (Norry and Fitton, 1983) are nearly absent in the As Sarat basalts. The overall abundances of the incompatible trace elements in the As Sarat basalts are low relative to values summarized by Camp and Roobol (1989) for continental alkali basalts, including other Red Sea rift-related basalts. In addition the As Sarat basalts are much less compatible-trace-element depleted (table 2; fig.9); average Ni and Cr values for flows of the CRS and for alkali olivine basalt of Harrat Rahat (Camp and Roobol, 1989) are 163 versus 122 and 376 versus 215, respectively.

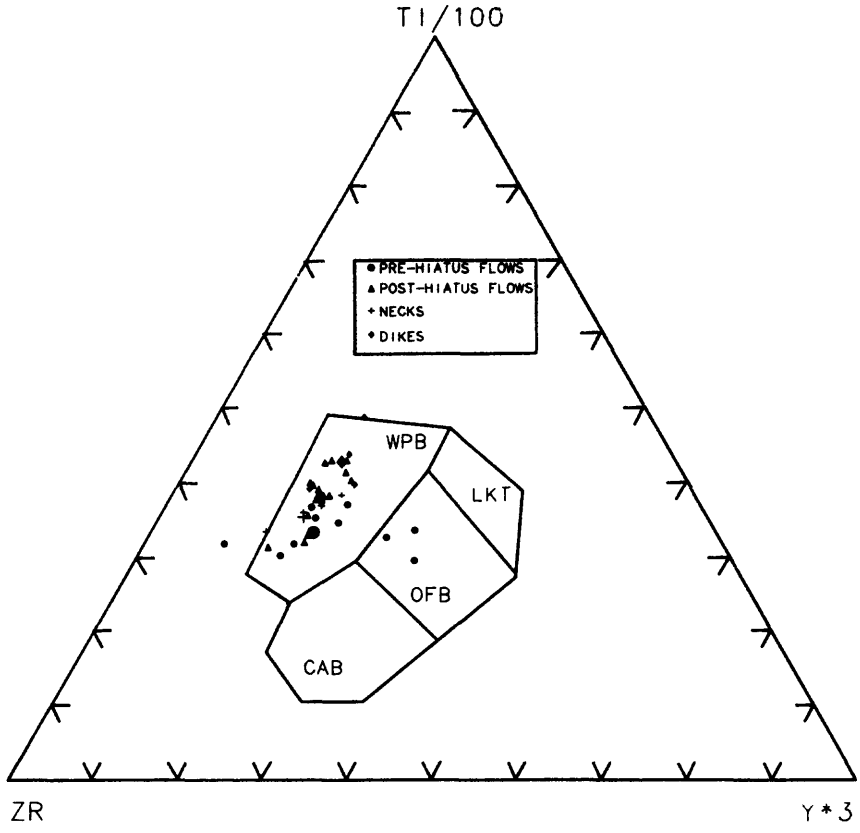


**Figure 7.**--Ternary diagram showing the proportions of Zr, Y, and Ti in samples of the As Sarat field. Enlarged plot symbols represent average compositions for rock type denoted by that symbol type. Field boundaries after Pearce and Cann (1973); WPB is within-plate basalt, LKT is low-potassium tholeiite, OFB is ocean-floor basalt, CAB is calc-alkali basalt.

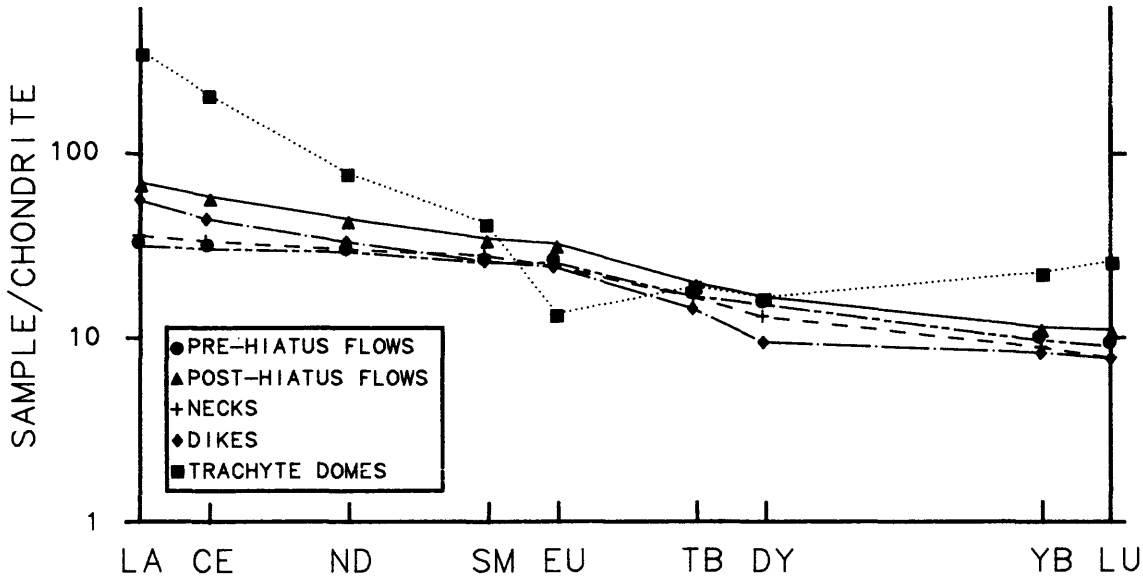


**Figure 8.**--Chondrite normalized REE plot showing average compositions of As Sarat field components.

**Table 4.**--Rare-element, uranium, and thorium analyses for selected samples as the As Sarat basalt field, Kingdom of Saudi Arabia. Hyphen indicates no data available.

| | Pre-hiatus basalt | | | Post-hiatus basalt | | | | Basalt neck | Basalt dike | Trachyte dome | MORB[1] | Lith[2] | Rahat[3] |
|---|---|---|---|---|---|---|---|---|---|---|---|---|---|
| Field No. | 112121 | 112120 | 112116 | 112109 | 112104 | 112420 | 112418 | 112087 | 112097 | 108557 | | | |
| | Chemical analyses, parts per million | | | | | | | | | | | | |
| La | 12 | 10 | 15 | 23 | 28 | 26 | 18 | 12 | 19 | 120 | - | 22 | 15.96 |
| Ce | 31 | 24 | 36 | 51 | 57 | 56 | 41 | 30 | 39 | 191 | 9.99 | 49 | 38.76 |
| Nd | 21 | 19 | 21 | 28 | 31 | 30 | 23 | 20 | 22 | 52 | 8.79 | 29 | 21.06 |
| Sm | 6.2 | 4.9 | 5.8 | 7.1 | 7.7 | 7.7 | 5.8 | 6.0 | 5.7 | 9.0 | 3.09 | 7.3 | 4.84 |
| Eu | 2.35 | 1.85 | 2.12 | 2.35 | 2.57 | 2.84 | 2.04 | 1.99 | 1.95 | 1.13 | 1.15 | 2.5 | 1.81 |
| Tb | 0.96 | 0.81 | 0.86 | 1.0 | 1.03 | 0.96 | 0.80 | 0.85 | 0.75 | 1.00 | - | 1.2 | - |
| Dy | 6.0 | 4.9 | 5.0 | 6.0 | 5.7 | 6.0 | 4.7 | 4.6 | 3.4 | 6.0 | - | 6.9 | 4.38 |
| Yb | 2.5 | 2.0 | 1.9 | 2.6 | 2.7 | 3.0 | 2.0 | 2.0 | 1.9 | 5.4 | 2.94 | 3.4 | 1.97 |
| Lu | .38 | .27 | .28 | 0.40 | 0.39 | .44 | .28 | .27 | .27 | 0.94 | - | 0.44 | 0.31 |
| Th | 1.0 | .7 | 1.2 | 2.1 | 2.3 | 2.3 | 1.8 | 1.1 | 2.1 | 30.0 | - | 2.6 | - |
| U | .3 | .3 | .5 | .7 | .7 | .6 | .6 | .3 | .9 | 8.0 | - | .7 | - |

1 Mid-ocean ridge basalt (Schilling, 1971)
2 Average of 9 analyses (sample numbers 165006, 165571, 165881, 175780, 165882, 165661, 175764, 175776, and 165767) presented by Pallister (1987) for Red Sea basalts from the central Arabian coastal plain
3 Alkali olivine basalt from Harrat Rahat (Camp and Roobol, 1989)

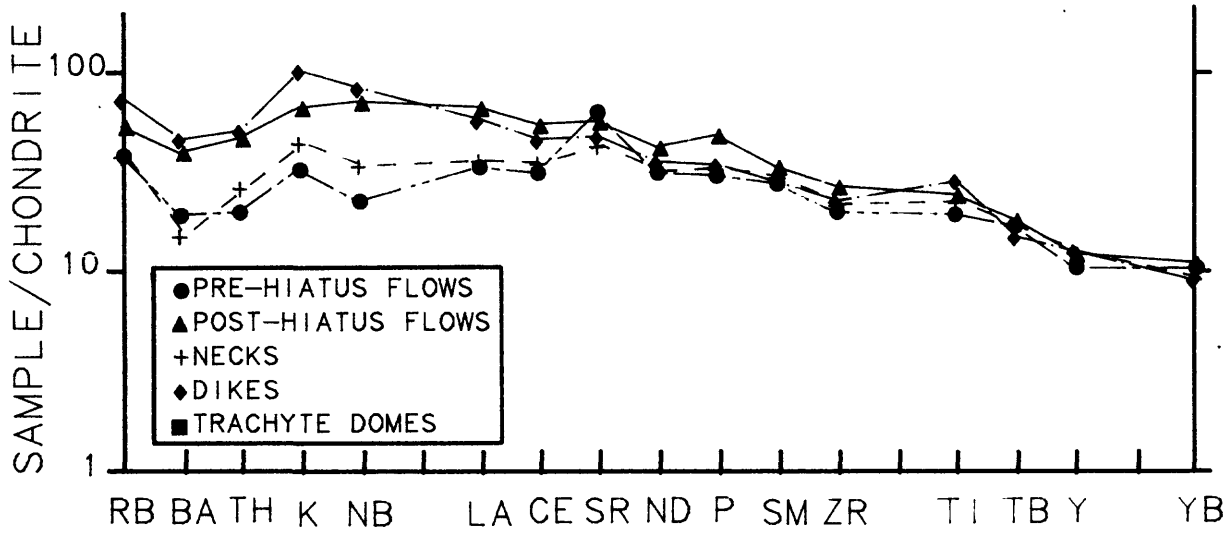


**Figure 9.**--Spidergrams showing average incompatible trace element abundances in As Sarat field components; normalized to chondrite values of Thompson and others (1983). Trace elements are in order of increasing incompatibility with mantle rocks; the most incompatible elements are on the left.

# Mineral Chemistry

Plagioclase phenocryst compositions were determined for 10 samples from the As Sarat field (table 5, fig. 10). Compositional zoning in plagioclase grains is minor, as indicated by core to rim analytical traverses and by small standard deviations computed from nine analyses per sample, except in samples 112108, 112105, and 112422, which have distinctly more calcic cores. Plagioclase compositions in flows of the CRS range from calcic andesine to sodic bytownite; the average composition is labradorite. Plagioclase compositions do not vary systematically with position in the CRS though they may vary systematically within single flows. Feldspars in the necks and dike are compositionally indistinguishable from those in flows of the CRS. Feldspars in the trachytes are anorthoclase.

Phenocryst and groundmass olivines were analyzed from nine As Sarat basalt samples (table 6). Phenocryst core compositions vary from Fo 86 to 77, and are zoned outward to lower Fo values at the rims that are similar to groundmass olivines. Groundmass olivines are not strongly zoned, but display considerable between sample variation (Fo 81-61). The calcium content of phenocryst cores is highly variable, but shows a systematic increase outward in the zoned rims.

Most of the As Sarat basalts contain olivine and plagioclase phenocrysts, but a few flows, dikes, and necks also contain clinopyroxene phenocrysts. Table 7 presents average analyses for both groundmass and phenocrystal clinopyroxene from nine samples. Clinopyroxenes in the As Sarat basalts display little between sample compositional variation or zoning within individual grains, and with one exception, are all titaniferous magnesian salites (fig. 11). Relic cores of a magnesian augite that occurs in dike sample 112094 (table 7) as well as the forsteritic olivine phenocryst cores (i.e. Fo 86-83) may represent xenocrystic phases or phenocrysts whose compositions represent equilibrium with melt in the source region.

**Table 5.**--Representative compositions of feldspar phenocrysts (except 112422) in rocks of the As Sarat volcanic field. Mean compositions and associated standard deviations (±) were calculated from nine (three analyses on each of three grains) analyses/sample.

| | Flow rocks | | | | | | Neck | Dike | Trachyte |
|---|---|---|---|---|---|---|---|---|---|
| Field No. | 112119 | 112111 | 112108 | 112105 | 112422 | 112415 | 112103 | 112094 | 108897 |
| $SiO_2$ | 52.97±1.76 | 50.54±0.85 | 55.18±5.19 | 56.45±2.88 | 54.23±3.84 | 50.57±0.41 | 52.94±1.69 | 51.06±0.60 | 66.39±0.48 |
| $Al_2O_3$ | 29.35±1.15 | 31.05±0.77 | 27.99±3.81 | 26.85±2.02 | 28.25±2.59 | 30.81±0.31 | 29.26±1.27 | 30.27±0.50 | 19.65±0.54 |
| FeO | 0.55±0.11 | 0.78±0.15 | 0.60±0.32 | 0.67±0.02 | 0.70±0.24 | 0.62±0.06 | 0.32±0.06 | 0.56±0.09 | 0.33±0.17 |
| CaO | 12.29±1.37 | 14.27±0.74 | 10.17±4.47 | 8.95±2.51 | 10.88±3.18 | 13.72±0.34 | 11.80±1.30 | 13.88±0.52 | .61±0.43 |
| $Na_2O$ | 4.44±0.70 | 3.27±0.35 | 5.28±1.81 | 5.95±1.10 | 4.83±1.58 | 3.48± .21 | 4.72±0.76 | 3.45±0.31 | 8.15±0.56 |
| $K_2O$ | 0.28±0.12 | 0.10±0.03 | 0.76±1.07 | 0.65±0.58 | 0.51±0.52 | 0.20±0.02 | 0.34±0.17 | 0.20±0.03 | 4.62±1.10 |
| Ab | 38.9 | 29.1 | 46.3 | 52.6 | 43.2 | 31.1 | 41.2 | 30.7 | 70.7 |
| An | 59.5 | 70.3 | 49.3 | 43.7 | 53.8 | 67.8 | 56.9 | 68.2 | 2.9 |
| Or | 1.6 | 0.6 | 4.4 | 3.8 | 3.0 | 1.2 | 2.0 | 1.2 | 26.4 |
| | labradorite | bytownite | andesine | andesine | labradorite | labradorite | labradorite | labradorite | anorthoclase |

**Table 6.**--Composition of olivines in rocks of the As Sarat volcanic field. Abbreviations used: Fo - forsterite component, Ca - Calcium in weight percent, W - total number of analyses per sample, N.O. - not observed in thin section.

| | 112119 Flow | 112117 Flow | 112111 Flow | 112108 Flow | 112105 Flow | 112422 Flow | B1 Flow | 112094 Dike | 112103 Neck |
|---|---|---|---|---|---|---|---|---|---|
| | | | | PHENOCRYSTS | | | | | |
| Fo range | 85.9-69.8 | 76.8-73.5 | 78.8-63.3 | 76.9-58.3 | N.O. | 83.4-67.6 | 86.3-73.2 | 84.8-80.7 | 83.9-68.7 |
| Fo ave. | 82.3 | 73.4 | 73.8 | 72.2 | | 74.6 | 81.4 | 83.4 | 79.6 |
| Ca range | 0.24-0.51 | 0.20-0.45 | 0.14-0.44 | 0.21-0.49 | | 0.24-0.47 | 0.20-0.32 | 0.19-0.28 | 0.13-0.30 |
| Ca ave. | 0.32 | 0.25 | 0.26 | 0.30 | | 0.33 | 0.25 | 0.23 | 0.21 |
| N | 31 | 9 | 12 | 10 | | 12 | 11 | 14 | 8 |
| | | | | GROUNDMASS | | | | | |
| Fo range | 71.6-61.1 | 74.6-62.5 | 59.4-57.6 | N.O. | 62.5-57.2 | 67.7-64.5 | 70.1-69.5 | 80.8-76.8 | 71.2-65.9 |
| Fo ave. | 66.6 | 67.7 | 58.6 | | 60.3 | 65.9 | 69.8 | 79.0. | 68.5 |
| Ca range | 0.50-0.59 | 0.28-0.57 | 0.40-0.52 | | 0.34-0.59 | 0.47-0.54 | 0.40-0.44 | 0.22-0.30 | 0.28-0.41 |
| Ca ave. | 0.55 | 0.43 | 0.47 | | 0.46 | 0.50 | 0.42 | 0.27 | 0.36 |
| N | 4 | 4 | 6 | | 6 | 3 | 2 | 4 | 9 |

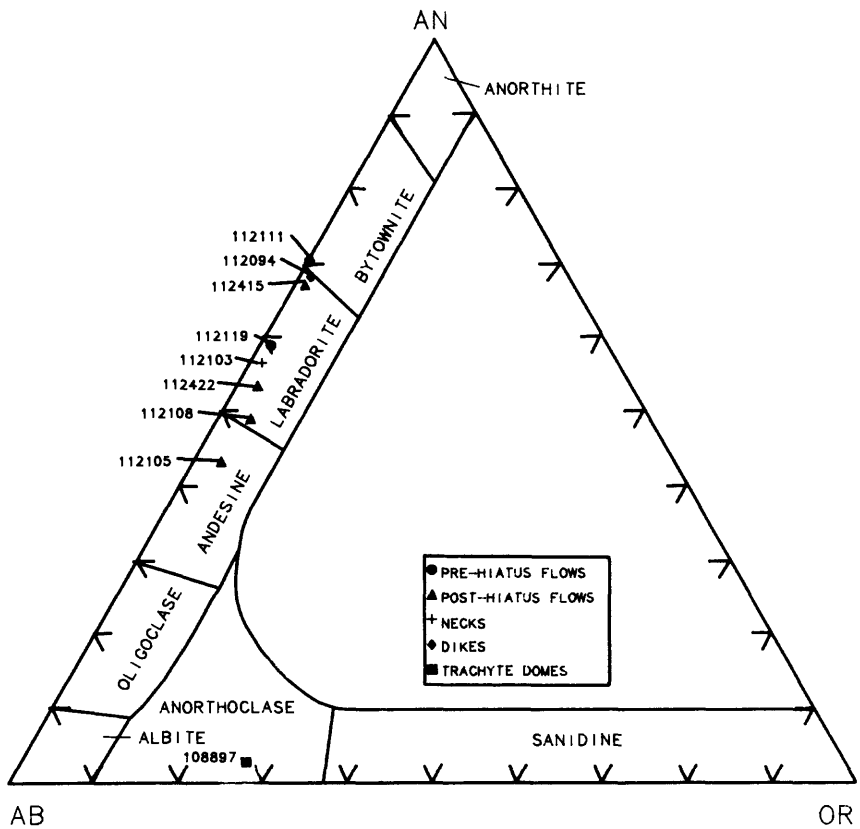


**Figure 10.**--Ternary diagram showing molecular proportions of feldspar end members in selected feldspars from rocks of the As Sarat field.

**Table 7.**--Compositions of clinopyroxenes in rocks of the As Sarat volcanic field. Mean oxide weight percent (m) and absolute standard deviation (sd) are presented. Total iron as FeO. Abbreciations: N, Number of analyses used for the average; WO, EN, and FS are the wollastonite, enstatite, and ferrosillite components, respectively.

| Sample No. | 112119 Flow Phenocryst | | 112119 Flow Groundmass | | 112111 Flow Groundmass | | 112108 Flow Phenocryst | | 112105 Flow Groundmass | | 112422 Flow Groundmass | |
|---|---|---|---|---|---|---|---|---|---|---|---|---|
| | m | sd | m | sd | m | sd | m | sd | m | sd | m | sd |
| $SiO_2$ | 49.19 | 1.48 | 50.30 | 1.71 | 50.05 | 0.90 | 50.22 | 1.10 | 50.58 | 0.30 | 51.00 | 0.41 |
| $TiO_2$ | 1.86 | 0.58 | 1.94 | 0.45 | 2.75 | .48 | 2.76 | 0.44 | 2.10 | .33 | 2.38 | .25 |
| $Al_2O_3$ | 4.94 | 1.45 | 4.94 | 1.32 | 4.16 | .64 | 4.41 | .63 | 2.69 | .36 | 4.42 | .40 |
| CaO | 22.09 | .49 | 21.44 | .92 | 20.98 | .34 | 21.21 | .25 | 20.80 | .52 | 20.94 | 2.0 |
| FeO | 7.89 | .92 | 7.88 | .79 | 8.92 | .21 | 8.30 | .32 | 8.68 | .21 | 7.51 | 3.0 |
| MgO | 13.33 | .88 | 13.09 | .69 | 12.79 | .52 | 12.92 | .48 | 11.87 | .15 | 13.29 | 2.6 |
| sum | 99.32 | | 99.58 | | 99.65 | | 99.83 | | 96.72 | | 99.53 | |
| N | 11 | | 14 | | 5 | | 9 | | 4 | | 8 | |
| WO | 47.2 | | 46.8 | | 45.9 | | 46.5 | | 47.2 | | 46.3 | |
| EN | 39.6 | | 39.7 | | 38.9 | | 39.4 | | 37.4 | | 40.8 | |
| FS | 13.2 | | 13.4 | | 15.2 | | 14.2 | | 15.4 | | 12.9 | |

| Sample No. | B1 Flow Groundmass | | 112103 Neck Groundmass | | 112094 Dike Relic Core | | 112094 Dike Phenocryst Rim | | 112094 Dike Groundmass | |
|---|---|---|---|---|---|---|---|---|---|---|
| | m | sd | m | sd | m | sd | m | sd | m | sd |
| $SiO_2$ | 49.20 | 1.48 | 50.27 | 0.60 | 50.82 | 0.61 | 46.26 | 1.76 | 46.60 | 2.10 |
| $TiO_2$ | 2.78 | 0.70 | 2.09 | .27 | 1.04 | .17 | 2.94 | 0.58 | 3.31 | 0.73 |
| $Al_2O_3$ | 5.09 | 1.65 | 3.94 | .77 | 6.69 | .52 | 8.20 | 2.30 | 7.24 | 2.32 |
| CaO | 20.93 | .40 | 22.52 | .34 | 17.73 | .50 | 21.73 | .76 | 22.37 | .60 |
| FeO | 7.04 | .67 | 7.21 | .13 | 6.92 | .23 | 7.48 | .33 | 8.22 | .51 |
| MgO | 13.39 | .86 | 13.80 | .22 | 16.11 | .52 | 12.19 | .90 | 12.25 | .91 |
| sum | 98.42 | | 99.82 | | 99.31 | | 98.80 | | 100.00 | |
| N | 2 | | 8 | | 4 | | 13 | | 5 | |
| WO | 46.5 | | 47.6 | | 38.9 | | 49.4 | | 48.8 | |
| EN | 41.3 | | 40.5 | | 49.2 | | 37.1 | | 37.2 | |
| FS | 12.2 | | 11.9 | | 11.9 | | 13.5 | | 14.0 | |

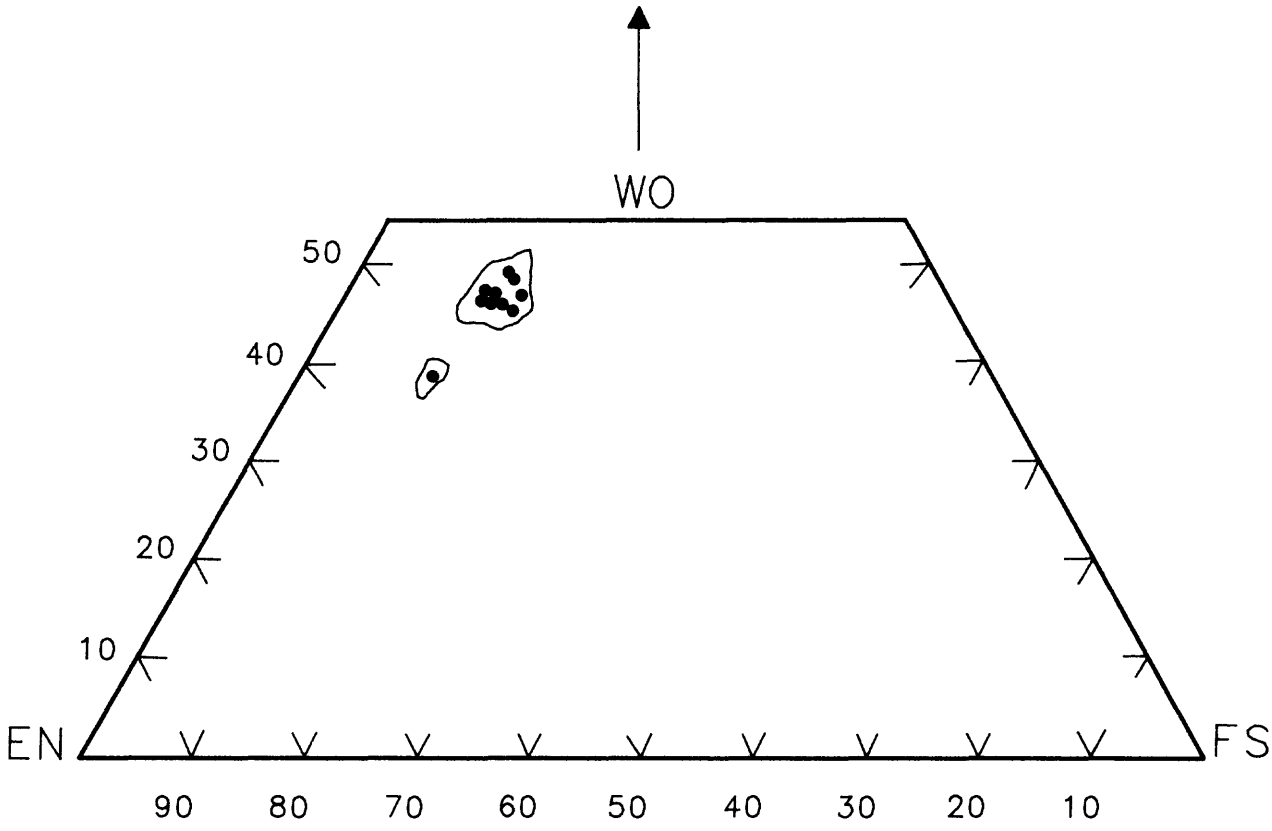


**Figure 11.**--Ternary diagram showing composition of clinopyroxene from As Sarat basalts. Dots show average compositions from table 7. The field boundaries show the limit of all data.

# PETROGENESIS AND TECTONIC SETTING

The change from subalkaline to alkaline basalt in the As Sarat field is significant and places certain constraints on the petrogenesis of these rocks. The invariant point in the basalt experimental system crosses the plane of silica saturation (fig. 12) as the pressure at which partial melting occurs increases (O'Hara, 1968). This relationship has been used to explain the coexistence of alkaline and subalkaline basaltic rocks in a single tectonic setting. As suggested by Pallister (1987) the occurrence of both alkaline and subalkaline basalt in association with Red Sea rift may result from partial melting of the mantle at various depths. In particular, the subalkaline pre-hiatus As Sarat basalts may represent partial mantle melting at approximately 2 GPa (20 kb, 70 km), whereas the alkaline, post-hiatus As Sarat basalts may represent melting at depths greater than 70 km (fig. 12). As Sarat basalts display some compositional deviation from the olivine-clinopyroxene cotectic (fig. 12); these deviations probably represent varying amounts of olivine ± clinopyroxene fractionation or accumulation (table 3).

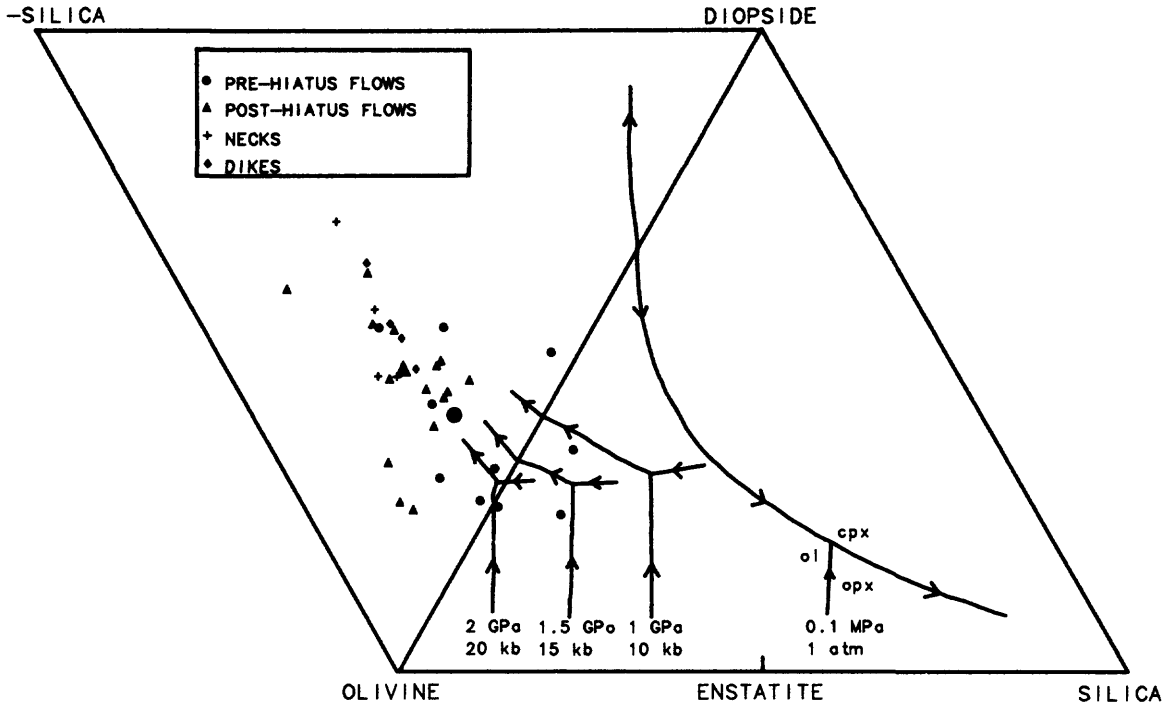


**Figure 12.**--Compositions of As Sarat basalt and liquidus phase relations for basaltic melts from Stolper (1980) and Walker and others (1979) projected from plagioclase on the diopside-olivine-silica saturation surface of the simplified basalt phase system using the methods of Walker and others (1979) and Pallister (1987). Enlarged plot symbols represent average compositions for rock type denoted by that symbol type.

REE abundances in pre-and post-hiatus basalt are similar, though LREE abundances in the post-hiatus basalts are almost double those in the pre-hiatus basalts, which suggests that all As Sarat basalt was produced by partial melting of chemically similar mantle material. $^{87}Sr/^{86}Sr$ ratios for three samples, from the base, middle, and top of the CRS, are 0.7034, 0.7033, and 0.7036, respectively (Coleman and others, 1977) and are consistent with oceanic mantle derivation (Faure, 1986). The absence of Nb anomalies, considered indicators of asthenospheric mantle partial melting (Thompson, 1986), in As Sarat basalts (fig. 9) suggests that they were generated from lithospheric mantle. Mantle-like initial strontium ratios and the absence of continental crustal xenoliths suggest little or no contamination of As Sarat basalt by evolved upper crustal rocks of the Precambrian basement.

Process identification diagrams use the geochemical behavior of incompatible and extremely incompatible elements to help determine whether partial melting, fractional crystallization, or a combination of these processes had dominant roles in basalt compositional evolution (Allegre and Minster, 1978; Minster and Allegre, 1978). Trace element abundance interrelationships in samples of As Sarat basalt (pre-and post-hiatus, necks and dikes) define steep linear regression lines (fig. 13

A-E) that trend toward the origin on these diagrams. Allegre and Minster (1978) and Minster and Allegre (1978) suggest that these characteristics indicate batch partial melting. Linear data arrays, (fig. 13 B, C in particular) on these plots indicate that As Sarat magmas experienced minimal subsequent crystal fractionation or accumulation. Increases in the abundances of incompatible elements, such as Ba and Zr, that accompany relatively minor MgO decreases indicate that varying degrees of partial melting played a dominant role in development of As Sarat compositional variation (table 2).

The major role of partial melting in the genesis of the As Sarat magmas is in contrast to processes identified as being responsible for compositional variation in volcanic rocks of Harrat Rahat (Camp and Roobol, 1989), the only other well studied Saudi Arabian Tertiary volcanic field. Composition data for rocks of Harrat Rahat indicate that partial melting was an essential but not the sole factor responsible for their compositional variation. Camp and Roobol (1989) suggest that Harrat Rahat magmas also experienced open-system fractionation. The age difference between Harrat Rahat rocks (10 Ma-present; Camp and Roobol, 1989) and As Sarat basalt (31-22 Ma), and the fact that different petrologic processes are inferred to have operated in the two systems suggest that the tectonic processes (rifting) responsible for extrusion of these rocks may also have been significantly different in the two areas.

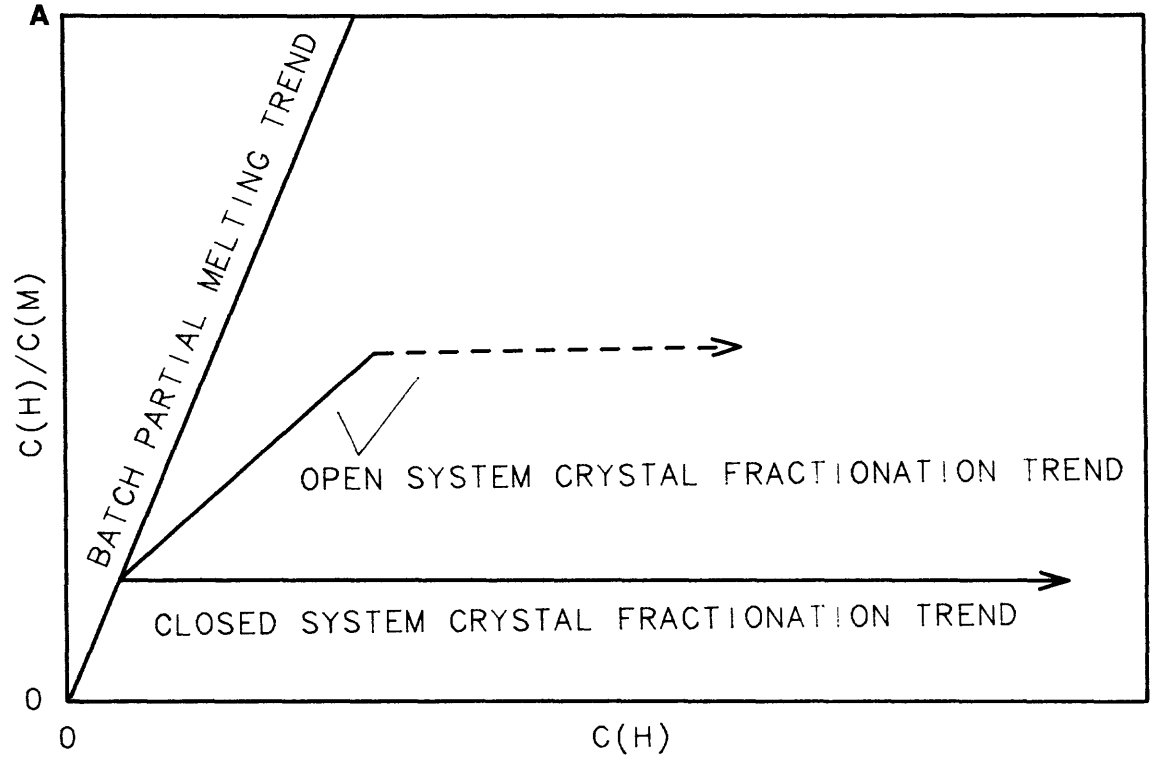


**Figure 13.**--Process identification trace element variation diagrams. **A**, theoretical, variation trends for different magmatic process (trend lines after Allegre and Minster, 1978); C(M) and C(H) are abundances of magmatophile and hypermagmatophile elements, respectively. **B-E**, variation diagrams for As Sarat basalt; solid lines are linear regression lines. Dashed fractionation trend lines, in **D** and **E**, from Camp and Roobol (1989) and Feigenson and others (1983), respectively.

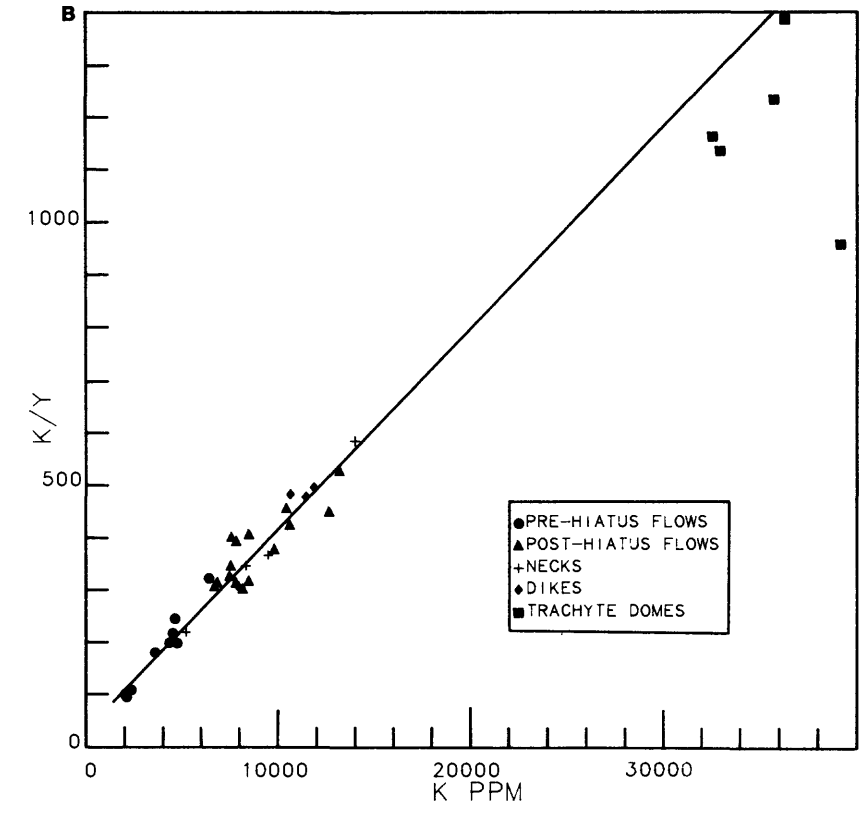


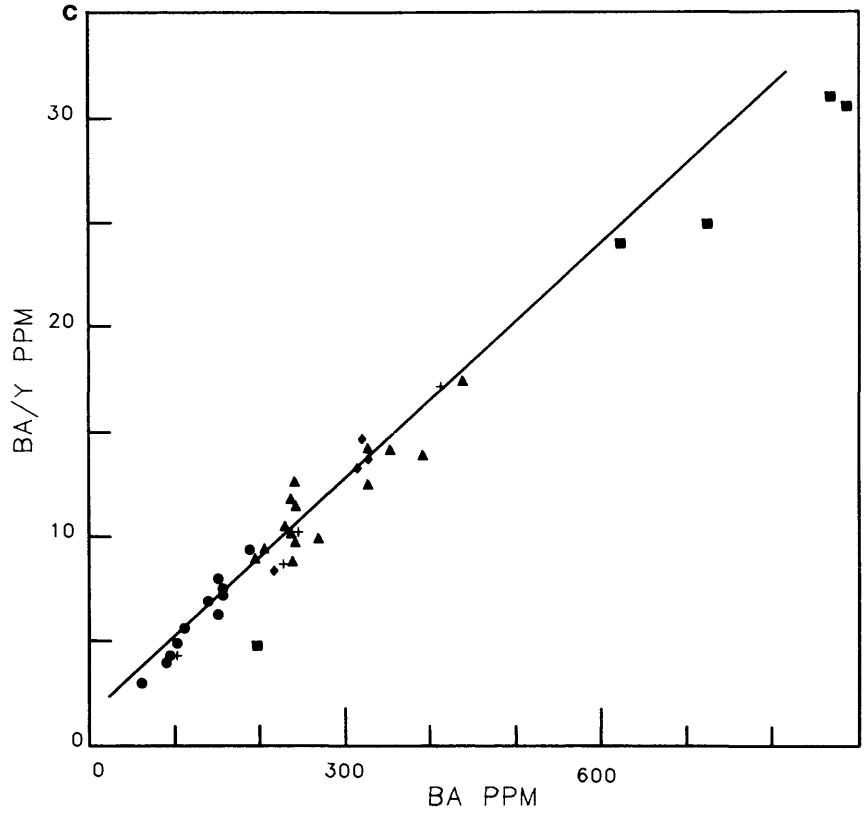


**Figure 13.--Process identification trace element variation diagrams--Continued**

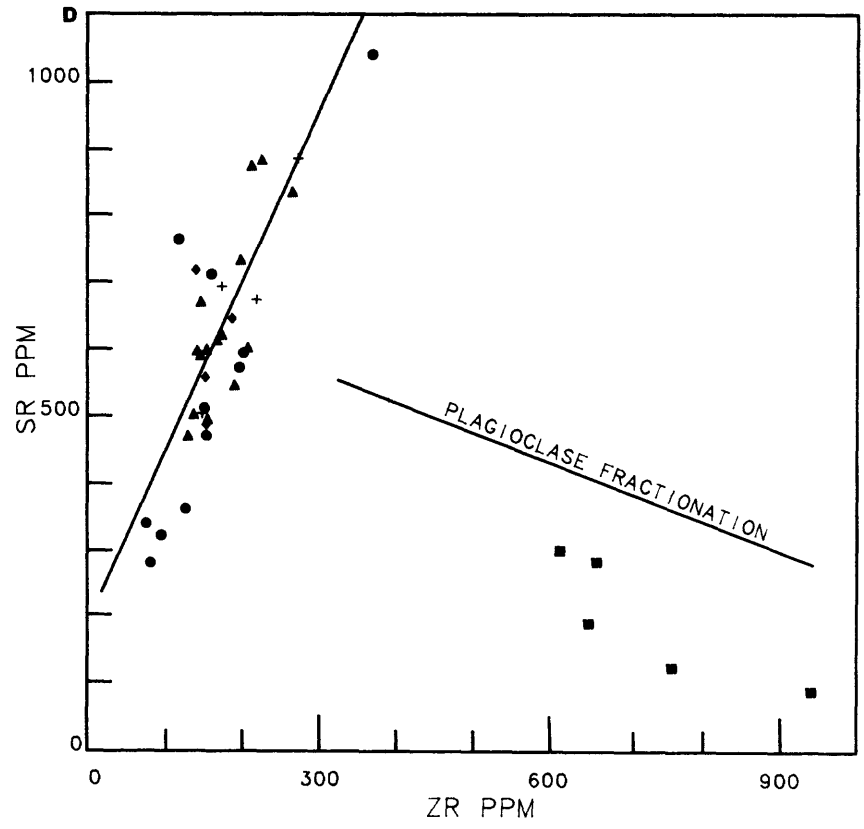


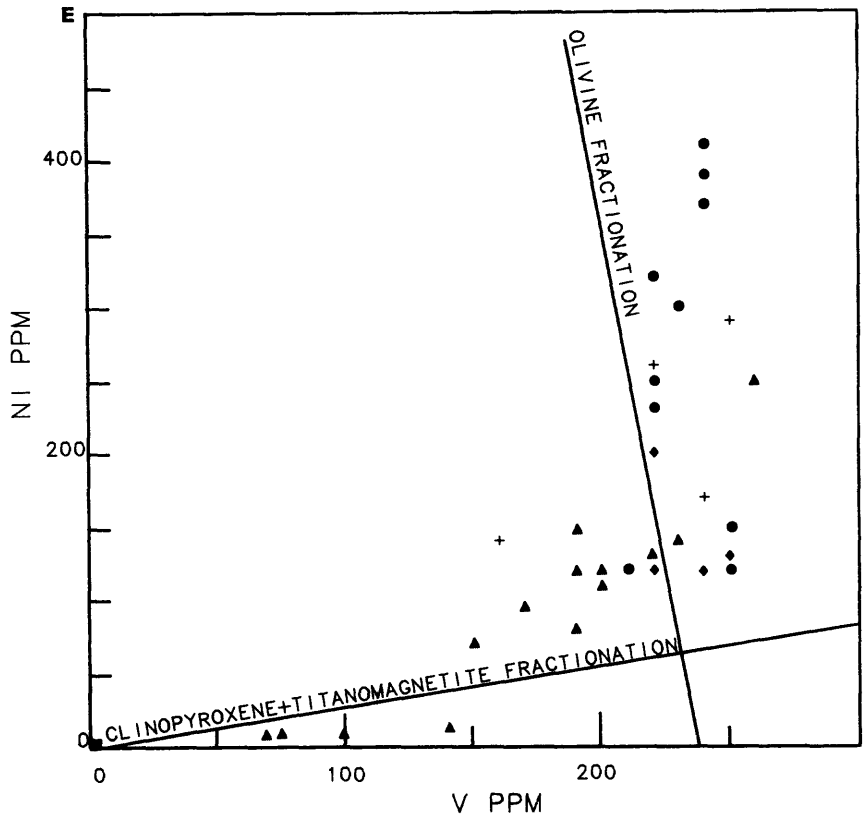


**Figure 13.--Process identification trace element variation diagrams--Continued**

Trace element abundances can be used to infer degrees of partial melting for a given igneous lithology. Given that bulk distribution coefficients for strongly incompatible trace elements are extremely low, the expression for Rayleigh melting reduces to $C_l/C_0 = 1/F$, where $C_l$ is the abundance of a trace element in the liquid, $C_o$ is its abundance in the source, and F is the fraction of partial melting (Shaw, 1970). Using this relation and assuming a mantle source that contains 1 ppm Rb (Frey and others, 1978), calculated partial melt percentages for the pre- and post-hiatus basalts, necks, and dikes are 8.3, 4.6, 4.0, 3.9, respectively. Assuming a mantle source that contains 15.5 ppm Zr (Frey and others, 1978), the same calculated partial melt percentages are 9.9, 8.8, 7.6, and 9.9, respectively. Post-hiatus basalt appears to represent a smaller percentage of partial melting than pre-hiatus basalt. The basalt necks and, less certainly, the dikes were generated by quantities of partial melting most similar to those characteristic of post-hiatus basalt.

REE abundances characteristic of the pre- and post-hiatus basalts are a function REE distribution coefficients. As suggested above, the post-hiatus basalts may represent a smaller degree of partial melting, which maximizes REE liquid abundances because the REE have small distribution coefficients in the environment of basalt genesis (Arth, 1976). The LREE are particularly incompatible in this environment (Arth, 1976) so that relatively smaller amounts of partial melting, such as that responsible for the post-hiatus basalts, will yield relatively LREE enriched liquids. Very modest positive Eu anomalies characteristic of the As Sarat basalts may result from the addition of a minor amount of feldspar (Hanson, 1980).

Polybaric crystal fractionation and(or) addition of phases had a minor role in development of As Sarat compositional variation. Their roles are most apparent in comparisons of As Sarat basalt compositions to compositions along the clinopyroxene-olivine cotectic (fig. 12). As Sarat basalts exhibit considerable deviation from cotectic compositions; these deviations are inferred to result from small amounts of olivine and(or) clinopyroxene fractionation. Covariation of major oxide and trace element abundances (table 3) substantiate the inference that some of the compositional variation is attributable to olivine and(or) clinopyroxene fractionation. Variation of some trace element abundances such as Ni and V (fig. 13E) also indicate that crystallization of olivine, clinopyroxene, and iron-titanium oxides contributed to As Sarat compositional variation. These features must be placed in the perspective offered by petrographic observations, however. Specifically, cumulate textures, megacrysts, and reaction textures have not been observed in As Sarat basalt, which implies that neither crystal fractionation nor accumulation occurred on a major scale.

The trachytes of the As Sarat field appear to have evolved from basalt by extensive fractionation, probably within a basaltic magma chamber. Plagioclase fractionation is well demonstrated by the large negative Eu anomaly that characterizes the trachyte REE pattern (fig. 8). Likewise, abundances of Sr and Zr (fig. 13D) indicate that plagioclase fractionation played a major role in derivation of

the trachytes from the basalt. Middle REE depletion in the trachyte may be a consequence of apatite fractionation; apatite is characterized by relatively elevated partition coefficients for the middle REE (Hanson, 1980). Compositional variation among the trachytes may be controlled by additional feldspar fractionation in addition to clinopyroxene and iron-titanium oxide fractionation (fig. 13D). Note that a large composition gap, between basalt and trachyte, exists in the As Sarat magmatic series for which intermediate members are not presently known, although several unsampled small "andesitic" intrusions mapped by Anderson (1979) in the southern part of the field may represent such rocks.

A tabulation of ages (Coleman and others, 1983; fig. 15) for spatially associated rocks of the Red Sea and Dead Sea rifts indicates that these volcanic rocks are approximately coeval. These ages are bimodally distributed which suggests that spreading at the Red Sea rift has been a two-stage process as first proposed by Girdler and Styles (1974). The first stage of magmatism began about 32 Ma and the second about 5 Ma. Volcanism during the first period was widespread and voluminous and led to the formation of the Trap Series or plateau volcanics that occur mainly in Ethiopia and Yemen, with minor extensions into Somalia and Saudi Arabia. In Ethiopia the bulk of the basaltic rocks were erupted between 32-15 Ma and 4.5-0 Ma (Jones, 1976; Mohr, 1983). The main Trap Series of the southern Yemen Arab Republic was formed in two stages between 30 and 19 Ma, with a hiatus between 26 and 23 Ma (Civetta and others, 1978). In northern Yemen and southern Saudi Arabia, the early basalts formed between 31 and 22 Ma (Coleman and others, 1983; Capaldi and others, 1983; present paper); evidence presented here indicates a hiatus at about 25-24 Ma. The appearance of basalt over a widespread area at about the same time (i.e. 31-30 Ma) suggests that these rocks, including the As Sarat basalts, formed during crustal thinning along the flanks of a zone of crustal extension in the southern Red Sea region (Coleman and others, 1983; Kellogg and Reynolds, 1983).

First stage rifting is approximately coeval with pre-hiatus As Sarat basalt, which was erupted between 31.1 and 25.2 Ma. Hempton (1987) and Bohannon and others (1989) suggest that spreading along the Red Sea rift ceased in response to a collision involving the Arabian and Eurasian plates. However, after 24 Ma magmatism continued in the region for another 6 m.y. The period between spreading episodes along the rift represents a time of regional plate reorganization in the Middle East that began about 25 Ma; renewed spreading did not begin again along the axis of the Red Sea rift until this reorganization was complete (about 5 Ma) and regionally coherent mantle flow was reestablished (Hempton, 1987). The effects of reorganization may have been complete somewhat earlier further south in the Ethiopia-Yemen region, however, as indicated by 10 Ma-old basalts. The chemical discontinuity between pre- and post-hiatus As Sarat basalt implies a change in the nature of magma genesis that is coincident with the beginning of this period of postulated regional plate reorganization.

# DATA STORAGE

All results obtained in this study are contained in this report therefore no Data File was established.

No updated information was added to the Mineral Occurrence Documentation System (MODS) data bank, and no new files were established.

# REFERENCES CITED


Allegre, C.J., and Minster, J.F., 1978, Quantitative models of trace element behavior in magmatic processes: Earth and Planetary Science Letters, 38, p. 1-25.

Anderson, R.E., 1979, Geology of the Wadi Atf (sheet 17/43 A) and Mayza (sheet 17/43 B) quadrangles, Kingdom of Saudi Arabia: Saudi Arabian Directorate General of Mineral Resources Bulletin 25, 33 p.

Arth, I.G., 1976, Behavior of trace elements during magmatic processes - a summary of theoretical models and their applications: U.S. Geological Survey Journal of Research, 4, p. 41-47.

Bohannon, R.G., Naesar, C.W., Schmidt, D.L., and Zimmermann, R.A., 1989, The timing of uplift, volcanism, and rifting peripheral to the Red Sea: A case for passive rifting?: Journal of Geophysical Research, 94, p. 1683-1701.

Camp, V.E., and Roobol, M.J., 1989, The Arabian continental alkali basalt province: Part I. Evolution of Harrat Rahat, Kingdom of Saudi Arabia: Geological Society of America Bulletin, 101, p. 71-95.

Capaldi, G., Manetti, P., and Piccardo, G.B., 1983, Preliminary investigation on volcanism of the Sadah Region (Yemen Arab Republic): Bulletin Volcanologique, 46, p. 413-427.

Chiesa, S., Civetta, L., De Fino, M., La Volpe, L., and Orsi, G., 1989, The Yemen Trap Series: genesis and evolution of a continental flood basalt: Journal of Volcanology and Geothermal Research, 36, p. 337-350.

Civetta, L., La Volpe, L., and Lirer, L., 1978, K-Ar ages of the Yemen Plateau: Journal of Volcanology and Geothermal Research, 4, p. 307-314.

Colby, J.W., 1968, Quantitative microprobe analysis of thin insulating films. Advances in X-ray Analysis, 11, p. 287-305.

Coleman, R.G., and McGuire, A.V., 1988, Magma systems related to the Red Sea opening: Tectonophysics, 150, p. 77-100.

Coleman, R.G., Fleck, R.J., Hedge, C.E., and Ghent, E.D., 1975, The volcanic rocks of southwest Saudi Arabia and the opening of the Red Sea: U.S. Geological Survey Open-File Report (IR)SA-194.

Coleman, R.G., Fleck, R.J., Hedge, C.E., and Ghent, E.D., 1977, The volcanic rocks of southwest Saudi Arabia and the opening of the Red Sea, *in* R.S. Hilpert (Editor) Red Sea Research 1970-1975: Saudi Arabian Directorate General of Mineral Resources Bulletin 22, p. Dl-D3O.

Coleman, R.G., Gregory, R.T., and Brown, G.F., 1983, Cenozoic volcanic rocks of Saudi Arabia: Saudi Arabian Directorate General of Mineral Resources Open-File Report USGS-OF-03-93, 82 p. U.S. Geological Survey Open-File Report 83-788.

Dalrymple, G.B., and Lanphere, M.A., 1969, Potassium-argon dating: San Francisco, California, W.H. Freeman, 258 p.

Elsass, F., and du Bray, E.A., 1982, Energy-dispersive X-ray fluorescence spectrometry with the Kevex 7000 system: Saudi Arabian Deputy Ministry for Mineral Resources Open-File Report USGS-OF-02-52, 53 p. On File at USGS Mission, Saudi Arabia

Engel, A.E.J., Engel, C.G., and Havens, R.G., 1965, Chemical characteristics of oceanic basalts and the upper mantle: Geological Society of America Bulletin, 76, p. 719-734.

Faure, G., 1986, Principles of isotope geology: New York, John Wiley and Sons, 589 p.

Feigenson, M.D., Hofmann, A.W., and Spera, F.J., 1983, Case studies on the origin of basalt: II. The transition from tholeiitic to alkalic volcanism on Kohala volcano, Hawaii: Contributions to Mineralogy and Petrology, 84, p. 390-405.

Frey, F.A., Green, D.H., and Roy, S.D., 1978, Integrated models for basalt petrogenesis: A study of quartz tholeiites to quartz melilitites from southeastern Australia using geochemical and petrological data: Journal of Petrology, 19, p. 463-513.

Girdler, R.W. and Styles, P., 1974, Two stage Red Sea floor spreading: Nature, 247, p. 7-11.

Hanson, G.N., 1980, Rare-earth elements in petrogenetic studies of igneous systems: Annual Review of the Earth and Planetary Sciences, 8, p. 371-406.

Hart, S.R., 1971, K, Rb, Cs, Sr, and Ba contents and initial Sr isotope ratios of ocean floor basalts: Philosophical Transactions of the Royal Society of London, Series A, 268, p. 573.587.

Hegner, E., and Pallister, J.S., 1989, Pb, Sr, and Nd isotopic characteristics of Tertiary Red Sea rift volcanics from the central Saudi Arabian coastal plain: Journal of Geophysical Research, 94, p. 7749-7755.

Hempton, M.R., 1987, Constraints on Arabian plate motion and extensional history of the Red Sea: Tectonics, 6, p. 687-705.

Ingamells, C.O., 1970, Lithium metaborate flux in silicate analysis: Analytica Chimica Acta, 52, p. 323-334.

Irvine, T.N., and Baragar, W.R.A., 1971, A guide to the chemical classification of volcanic rocks: Canadian Journal of Earth Sciences, 8, p. 523-548.

Jackson, L.L., Brown, F.W, and Neil, S.T., 1987, Major and minor elements requiring individual determination, classical whole rock analysis, and rapid rock analysis, *in* P.A. Baedecker (Editor), Methods for Geochemical Analysis: U.S. Geological Survey Bulletin 1770, p. G1-G23.

Jones, P.W., 1976, Age of the lower flood basalts of the Ethiopian plateau: Nature, 261, p. 567-569.

Kellogg, K.S., and Reynolds, R.L., 1983, Opening of the Red Sea: constraints from a paleomagnetic study of the As Sarat volcanic field, southwestern Saudi Arabia: Geophysical Journal of the Royal Astronomical Society, 74: 649-665.

Le Bas, M.J., Le Maitre, R.W., Streckeisen, A., and Zanettin, B., 1986, A chemical classification of volcanic rocks based on the total alkali-silica diagram: Journal of Petrology, 27, p. 745-750.

Lichte, F.E., Golightly, D.W., and Lamothe, P.J., 1987, Inductively coupled plasma-atomic emission spectroscopy, *in* P.A. Baedecker (Editor) Methods for Geochemical Analysis: U.S. Geological Survey Bulletin 1770, p. B1-B10.

McGuire, A.V., and Bohannon, R.G., 1989, Timing of mantle upwelling: Evidence for a passive origin for the Red Sea Rift: Journal of Geophysical Research, 94, p. 1677-1682.

McKee, E.H., and Elston, D.P., 1980, Reversal chronology from a 7.9- to 11.5-M.Y.-Old volcanic sequence in central Arizona: Comparison with ocean floor polarity record: Journal of Geophysical Research, 85, p. 327.337.

Minster, J.F., and Allegre, C.J., 1978, Systematic use of trace elements in igneous processes: Part III. Inverse problem of batch partial melting in volcanic suites: Contributions to Mineralogy and Petrology, 68, p. 37-52.

Mohr, P., 1983, Ethiopian flood basalt province: Nature, 303, p. 577-584.

Mohr, P., and Zanettin, B., 1989, The Ethiopian flood basalt province, *in* J.D. Macdougall (Editor), Continental Flood Basalts: Kluwer Academic Publishers: Dordrecht, Netherlands, p. 63-110.

Norry, M.J., and Fitton, J.G., 1983, Compositional differences between oceanic and continental basic lavas and their significance, *in* C.J. Hawkesworth and M.J. Norry (Editors), Continental basalts and mantle xenoliths: Cheshire, England, Shiva Publishing, Ltd. p. 5-19.

O'Hara, M.J., 1968, The bearing of phase equilibria studies on the origin and evolution of basic and ultrabasic rocks: Earth Science Reviews, 4, p. 69-133.

Overstreet, W.C., Stoeser, D.B., Overstreet, E.F., and Goudarzi, G.H., 1977, Tertiary laterite of the As Sarat Mountains, Asir Province, Kingdom of Saudi Arabia: Saudi Arabian Directorate General of Mineral Resources Bulletin 21, 30 p.

Pallister, J.S., 1987, Magmatic history of Red Sea rifting: Perspective from the central Saudi Arabian coastal plain: Geological Society of America Bulletin, 98, p. 400-417.

Pearce, J.A., and Cann, J.R., 1973, Tectonic setting of basic volcanic rocks determined using trace element analyses: Earth and Planetary Science Letters, 19, p. 290-300.

Ringwood, A.E., 1975, Composition and petrology of the Earth's mantle: New York, McGraw Hill, 618 p.

Schilling, J.G., 1971, Sea-floor evolution: Rare-earth evidence: Philosophical Transactions of the Royal Society of London, Series A, 268, p. 663-706.

Shaw, D.M., 1970, Trace element fractionation during anatexis: Geochimica et Cosmochimca Acta, 34, p. 237-259.

Steiger, R.H., and Jager, E., 1977, Subcommission on geochronology: Convention on the use of decay constants in geo- and cosmochronology: Earth Planet Letters, 36, p. 359-362.

Stoeser, D.B., 1984, Reconnaissance geology of the Wadi Tarib quadrangle, sheet 18/43 C, Kingdom of Saudi Arabia: Saudi Arabian Deputy Ministry for Mineral Resources Technical Record USGS-TR-04-4, 77 p. On file at the USGS Mission Saudi Arabia.

Stolper, E., 1980, A phase diagram for mid-ocean basalts: Preliminary results and implications for petrogenesis: Contributions to Mineralogy and Petrology, 74, p. 13-27.

Tabor, R.W., Mark, R.K., and Wilson, R.H., 1985, Reproducibility of the K-Ar ages of rocks and minerals: An empirical approach: U.S. Geological Survey Bulletin 1654, 5 p.

Taggart, J.E., Jr., Lindsay, J.R., Scott, B.A., Vivit, D.V., Bartel, A.J., and Stewart, K.C., 1987, Analysis of geologic materials by X-ray fluorescence spectrometry, *in* P.A. Baedecker (Editor), Methods for Geochemical Analysis: U.S. Geological Survey Bulletin 1770, p. E1-E19.

Thompson, R.N., 1986, Sources of basic magmas: Nature, 319, p. 448-449.

Thompson, R.N., Morrison, M.A., Dickin, A.P., Hendry, G.L., 1983, Continental flood basalts ... Arachnids rule OK?, *in* C.J Hawkesworth and M.J. Norey (Editors), Continental basalts and mantle xenoliths: Cheshire, England, Shiva Publishing, Ltd., p. 158-185.

Walker, D., Shibata, T., and DeLong, S.E., 1979, Abyssal tholeiites from the Oceanographer fracture zone: II. Phase equilibria and mixing: Contributions to Mineralogy and Petrology, 70, p. 111-125.